Spring 1-1-2013

Validation of an Ion Optics Software Model against the DANDE Wind & Temperature Spectrometer

Kyle Dux Kemble
University of Colorado at Boulder, kyle.kemble@colorado.edu

VALIDATION OF AN ION OPTICS SOFTWARE MODEL AGAINST THE DANDE WIND & TEMPERATURE SPECTROMETER

by

KYLE DUX KEMBLE

B.S., University of Colorado Boulder, 2011

A thesis submitted to the

Faculty of the Graduate School of the

University of Colorado in partial fulfillment

of the requirement for the degree of

Masters of Science

Department of Aerospace Engineering Sciences

2013

This thesis entitled:
Validation of an Ion Optics Software Model against the DANDE Wind & Temperature Spectrometer
written by Kyle Dux Kemble
has been approved for the Department of Aerospace Engineering Sciences

_____
Dr. Scott E. Palo

_____
Dr. Marcin D. Pilinski

Date_____

The final copy of this thesis has been examined by the signatories, and we
Find that both the content and the form meet acceptable presentation standards
Of scholarly work in the above mentioned discipline.

Kemble, Kyle Dux (M.S., Aerospace Engineering Sciences)

Validation of an Ion Optics Software Model against the DANDE Wind & Temperature Spectrometer

Thesis directed by Associate Professor Scott E. Palo

The Drag & Atmospheric Neutral Density Explorer (DANDE) is slated for launch in the first half of 2013 into a highly eccentric near polar orbit to study the neutral thermosphere. It is a 50kg ~0.45m diameter spherical payload that will attempt to make measurements of the drag forces on spacecraft in LEO between 200-400km altitude and simultaneously sample the composition, thermal energy, and wind vector of the atmosphere. These two measurements together on a single platform will offer greater spatial and temporal detail to space weather measurements in this region on a single low-cost platform. This will be done with a sub-μg resolution accelerometer suite designed and built at the University of Colorado at Boulder. Complementary measurements by a Wind & Temperature Spectrometer (WTS) developed in part with Goddard Space Flight Center will gather information of the wind vector and atmospheric composition.

This work focuses primarily on the WTS instrument and the operational considerations levied on it through analysis of proto-flight and flight testing results. Additionally an ion optics modeling software is utilized called SIMION to take these empirical results and form a test correlated model of the instrument. The process for validation of the instrument behavior in SIMION is outlined by first identifying the performance metrics of the final instrument and running a similar testing campaign on the simulate instrument. The performance components in question are the relation the Small Deflection Energy Analyzer (SDEA) voltage to particle energy called the SDEA Plate factor observed at 3.6eV/V. The energy resolution of the system, or its ability to differentiate between selected energies and unselected energies which is ~7% of the overall sampled species. Finally for consideration is the overall selection efficiency of the instrument across an energy spectra within the SDEA chamber, lower selection efficiency will result in less overall observable particles reducing the signal to noise ratio. These metrics can then lend to operational considerations for the impending flight of DANDE.

Dedication

To all of my family and friends for the support that I have received in the long road leading up to preparing this work, I could have never done it without you.

Everyone at the Colorado Space Grant Consortium and Aerospace Engineering Sciences Department that made DANDE a possibility for me to work on and study for the past six years.

Acknowledgements

The author would like to take a moment to recognize the people who aided in the technical development and enabled this research to be possible.

Dr. Scott Palo for is advising and mentorship through this research as well as always being a sounding board to help overcome the hurdles we faced as we finished the DANDE satellite program.

Dr. Marcin Pilinski for getting me involved in DANDE during my undergraduate studies and maintaining his personal time investment of DANDE after finishing his studies.

Dr. David Voss for the energy he brought to the University NanoSatellite Program and always providing a clear level head throughout closeout of the satellite in preparation for launch.

Chris Koehler & Brian Sanders for taking a chance in hiring me as a freshman at the Colorado Space Grant Consortium opening the door to countless opportunities for growth and launching my career.

Caitlyn Cooke & Rees McNally for the tireless days we spent together during the final push to delivery with the commitment to making DANDE work not just once but every time.

To the entire DANDE student team past, present, and future for endowing this program with the awe inspiring spirit of something greater than ourselves that it has come to embody. Without the countless hours committed to the program the satellite would have never converged and become the reality that it is today.

CONTENTS

TABLES

FIGURES

CHAPTER 1: INTRODUCTION

1.1 Motivation

The Drag and Atmospheric Neutral Density Explorer (DANDE) is a 50kg microsatellite being developed by students at the Colorado Space Grant Consortium in partnership with the Department of Aerospace Engineering Sciences at the University of Colorado Boulder. Its primary function is to study the space weather environment in Low Earth Orbit (LEO) in an effort to understand how density perturbations are changing the atmospheric drag forces on spacecraft in the region. The flight space vehicle is shown in Figure 1, on the left is an image of the flight system taken during environmental testing, and right is a cutaway CAD model of the spacecraft with callouts for main subsystems and instruments.

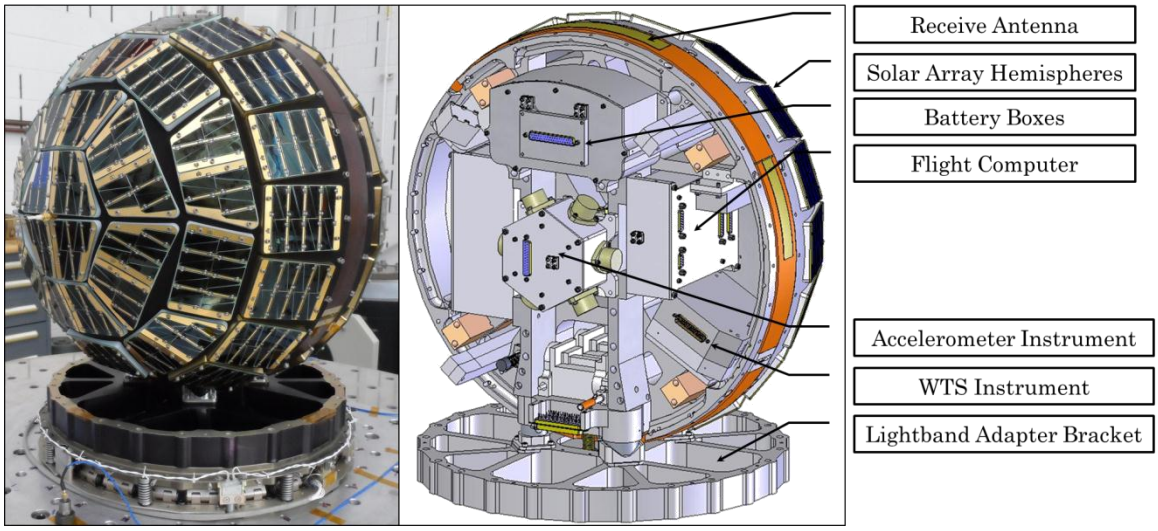

Figure 1 (LEFT) DANDE Spacecraft (RIGHT) Cutaway CAD Model

To accomplish its the satellite has two instruments on board discussed in chapter 2, the first a sub-μg precision accelerometer instrument that measures the along track accelerations of the spacecraft. Acceleration measurements are generated from

spacecraft rotation and six navigation grade accelerometers which are pointed into and out of the drag vector and can be combined to estimate the forcing on the spacecraft. The second instrument onboard is a Wind & Temperature Spectrometer (WTS), used to directly sense the atmospheric constituents, kinetic temperature and bulk velocity. This second instrument is the point of discussion for this work since it requires specialized facilities for testing and characterization. Also related to the science mission is the spacecraft geometry itself, it is of a non-traditional spherical shape. This geometry allows for a near constant drag area projected to the atmosphere regardless of spacecraft attitude, this would then translate into a near uniform forcing and ultimately acceleration on the spacecraft which is a direct science objective to capture. From the method of acceleration data capture the system rotates about the apex of the solar hemispheres causing each one of the sensing heads to be pointed into the ram vector and π radians later anti-ram. The WTS in turn is able to sample in all attitude states to build up a full 3D wind vector profile.

Characterization of the WTS involves a testing suite at hard vacuum ($<10^{-5}$ torr) pressures to identify not only final flight performance, but ideally determining sensitivities related to instrument geometry. To perform these measurements a well understood ion source needs to be present that can inject uniform and varying energy ions into the instrument for data collection. The nature of DANDE being a student mission made this reality cost prohibitive since a vacuum chamber was not readily available nor is it completely feasible to expect several sets of varying ion

optics geometry parts to be run through a gauntlet of tests. Flight instrument testing was carried out at Goddard Space Flight Center as well as Lockheed Martin, but these series of test were only capable of determining operation characteristics less the envelop of the instrument performance. These data sets can provide a basis for a test correlated model of the instrument to further investigate its performance outside of empirical testing. SIMION was previously being evaluated as a tool for ion optics modeling. By the nature of WTS being an ion optics instrument to study the energy spectrum only end to end measurements can be made, however the power of having a workbench like SIMION is that internal instrument properties can be studied in greater detail. The way this tool approaches the problem is to create multiple potential arrays that can have user defined voltages associated and simulate the trajectory of ions through the fields. It is also capable of magnetic field modeling, but for the purposes of the DANDE WTS there are no magnetic fields actively used in particle selection and detection.

SIMION has been identified as an electric and magnetic field modeling software package capable of replicating the DANDE WTS data products for further characterization outside of the lab. The exercise of building up a WTS model and comparing it to the know results of testing has distinct benefits, one the data products from the simulated instrument can be fed as an input to tools for data inversion effectively testing the ground processing capabilities to make density and winds measurements. And two for future iterations of the WTS instrument understanding the key geometric sensitivities in energy selection and efficiencies

can be harnessed to further bound the trade-space when designing to future missions.

The paradigm that is presented with DANDE of having performance data of the system, but the desire to create an encompassing system model allows for a verification of SIMION as modeling tool for the future while expanding the knowledge base of the current flight instrument which will directly impact flight operations. Not all resources gathered to support arguments for modeling or observed performance are under the direct purview of this work. Testing data of the flight instrument for DANDE comes via the DANDE program run out of the Colorado Space Grant Consortium. Additionally cursory evaluation of SIMION as a modeling tool stems from an independent study in the Aerospace Engineering Sciences Department. A particular challenge then is incorporating these different sources to build an argument for a comprehensive model being rooted in reality.

SIMION validation of simple geometries against an analytic solution provides a basis to model the more complex geometry of the DANDE WTS and infer that solutions are real. Comparing performance metrics of the WTS instrument from chamber testing to SIMION then acts as further support to a software model replicating the flight instrument. With agreement between truth data and SIMION results further investigation into the behavior of the system from parameters that were not tested to those which were not observable ultimately providing insight into on orbit considerations as well as technical changes for future revisions of the instrument.

1.2 Scope

For the purposes of this work there are four major objectives to be completed and assessed, these objectives can be summarized by the following:

- Comprehensive understanding of the DANDE system and operations.
- Evaluation of existing datasets for WTS from previous testing.
- Ion Optics modeling assessment in SIMION.
- Operational considerations levied onto DANDE in light of modeling.

The first two objectives are a collaboration that involves several students at the Colorado Space Grant Consortium and their direct participation on the DANDE program. My responsibility in this process is to collect and analyze this data in an effort to distill down to key evaluation metrics of performance. The metrics should be transferable to the software model in SIMION to evaluate the reliability of recreating the WTS instrument performance. After creating an argument for the software model agreement with physical data operational considerations should be generated and assessed against the DANDE space vehicle operations concept to ensure the spacecraft can meet its mission objectives of spatially and temporally relevant space weather measurements.

CHAPTER 2: BACKGROUND

2.1 The DANDE Mission Background

DANDE is a 50kg 0.45m diameter spherical satellite. Its primary mission is to measure atmospheric density. This is done by measuring the quantities such as mass, acceleration, cross-sectional area and winds which are fed into the equations of motion governing atmospheric drag shown in Equation 1:

$$\vec{F} = m\vec{a} = {}^{1}/_{2}\,\rho A\left(\vec{V}_{sc} + \vec{V}_{w}\right)^{2} \qquad \text{Equation 1}$$

The variables in Equation 1are the acceleration of the spacecraft (a), atmospheric density (ρ) and two velocity terms, the spacecraft velocity (V_{SC}) and the wind velocity (V_w). The sum of this vector quantity results in the total atmospheric velocity with respect to the spacecraft. This forcing on all LEO satellites is dictated by the overall geomagnetic activity which can vary due to energy transfer from solar output and predominantly storms. In the grand scheme of things fluctuations in this forcing will perturb the orbits of all satellites and it can become a large man power effort to maintain the orbit tracks for all catalogued objects. Studying the space weather environment is operationally useful to scientists around the globe as well as those cataloging the orbits of spacecraft. All measurements stem from making inroads to study parameters of Equation 1 and different spacecraft can be characterized as purpose built or making opportunistic measurements of these phenomena. A small cross section of space weather monitoring spacecraft from the dawn of the space age to the present are shown in Figure 2 noting which measurements are be taken on the respective platforms along with DANDE. Where

DANDE makes its mark is by trying to obtain these measurements on a purpose built spacecraft that largely makes observations of all the metrics available for study except for pressure. The desired operations concept would be to observe the lower thermosphere from 400km down to 200km at a very dynamic part of the atmosphere near end of life for many spacecraft.

mission	date	Accel. /Drag	composition	pressure	cross-track winds	in-track winds	large structure	small structure	temp.	C_D
AE 	1960s		■	■						
Cannon Ball 	1960s	■	■							
DE 	1970s		■	■	■	■	■	■	■	
SAN MARCO 	1960s -1980s	■	■		■	■	■		■	
S3-1 	1980s	■	■	■						
CHAMP 	2000s - present	■			■		■	■		
GRACE 	2000s - present	■			■		■	■		
ANDE 	~2009		■		■		■			■
DANDE 	~2010 ~2011	■	■		■	■	■	■	■	■

Figure 2 Historical Catalogue of Space Weather Monitoring Satellites [5]

The list in Figure 2 is by no means comprehensive, but serves to describe the general characteristics of payloads. Earlier measurements of thermosphere density perturbations come from spacecraft that were intent on studying the atmosphere as a primary objective. Some of the more recent data sources like CHAMP and GRACE are missions to study the ionosphere and gravity fields, but to make their measurements have highly sensitive accelerometers onboard to remove external accelerations from gravity measurements [6]. The accelerometers fundamentally

are measuring atmospheric drag perturbations to the spacecraft and can be used as a data source for drag as well as winds, but at the lack knowledge for composition and temperature. DANDE becomes a unique figure with its novel approach to sense the acceleration at the same time as collecting the composition and winds and further doing so over shorter time scales. But it also has a simplified spherical geometry to reconcile composition measurements resulting in density estimates to drag accelerations which will act on the spacecraft more or less uniformly despite a changing attitude state [5]. To accomplish its mission goals DANDE will rotate navigation grade accelerometers into and out of the velocity vector while the WTS aperture will scan through the full rotation of the spacecraft as shown in Figure 3.

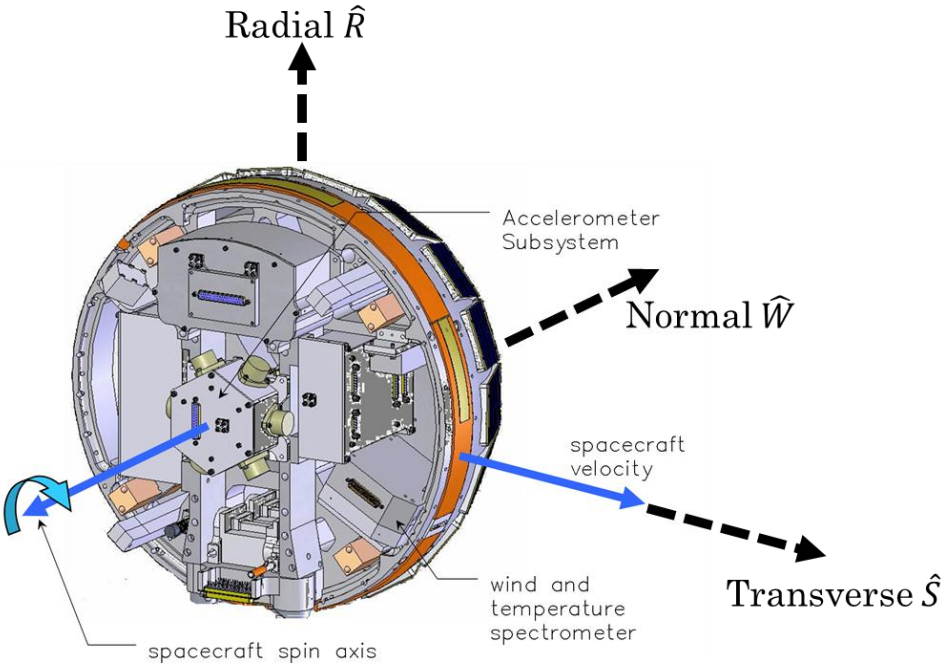

Figure 3 Spacecraft instruments in relation to the spacecraft orbit reference frame

In this graphic the accelerometers are called out and their sensing axis will rotate in and out of the spacecraft velocity vector about orbit normal. The WTS instrument

aperture will scan through the full rotation of the spacecraft providing data products in the ram vector as well as each orthogonal point in the arc. The rotation rate is levied by the accelerometers to be in a low noise portion of its PSD, so ultimately the final design calls for a rate of 10 rpm. The dashed lines represent the spacecraft local reference frame on orbit.

Currently DANDE is anticipating a launch in the first half of 2013 to an approximately 1500km x 325km orbit with an inclination of 80°. This orbit will provide the potential for atmospheric profiling as the spacecraft dips into the atmosphere and climbs back out. As the orbit decays the perigee of the orbit will drop further into the atmosphere allowing for measurements deeper into the thermosphere. The primary range of interest is 400km down to 200km for scientific study which will nominally allow for 15 minutes per orbit of data collection at these altitudes. It also scopes scientific data collection efforts to specific periods of the orbit, which can help the student mission developed more pointed science objectives. The hardware was delivered to the Air Force Research Laboratories University Nanosatellite Program (UNP) for environmental testing in the summer of 2012, and completed its host environmental testing by April 2013. Regrettably hardware testing with the WTS instrument has since raised greater questions as to the operations of the instrument on orbit, this provides further motivation for this work since the hardware is not present to be sent through vacuum characterization. However there is sufficient data to aid in the creation of this software model to further refine the operations concept for WTS on orbit.

2.2 Accelerometer Measurements Overview

The accelerometer instrument suite consists of six commercial off the shelf accelerometer heads (Honeywell QA-2000) and analog circuitry to amplify the subtle acceleration (sub μg) signal due to atmospheric drag. By the nature of spinning the entire spacecraft and orienting the accelerometers such that their individual sense axes form a plane perpendicular to the spin vector the acceleration signal is not a constant DC signal but a modulated cosine function. The spin rate of DANDE was selected such that is occurs in a region where the noise levels from the accelerometer are a minimum, as shown in Figure 4. Operating in this region of the accelerometer performance curve will serve to maximize the signal to noise ration of the acceleration measurements.

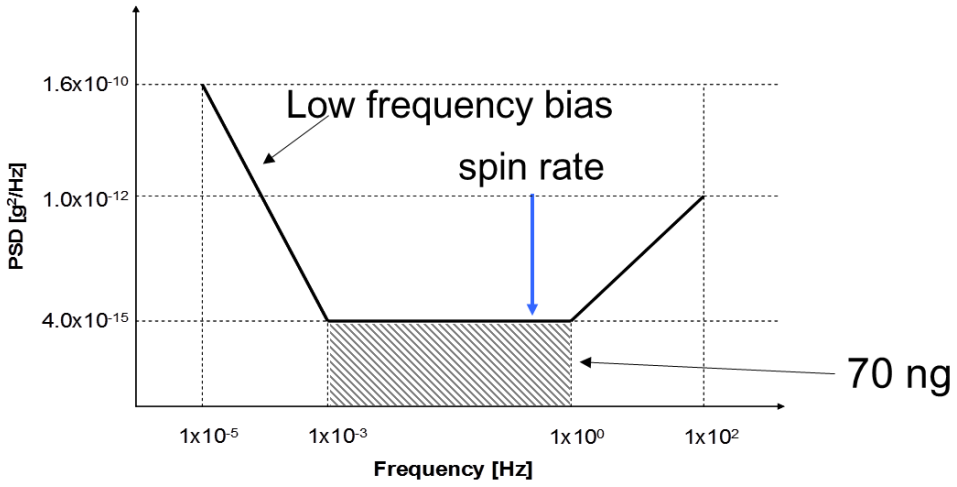

Figure 4 DANDE Accelerometer Spectral Noise Content

Because DANDE is spinning, the acceleration parallel and then some time later in the spin antiparallel (~3 seconds) to the velocity vector can effectively be utilized as a self-calibration for any observed low-frequency biases in the measurements. This conceived output is graphically represented in Figure 5.

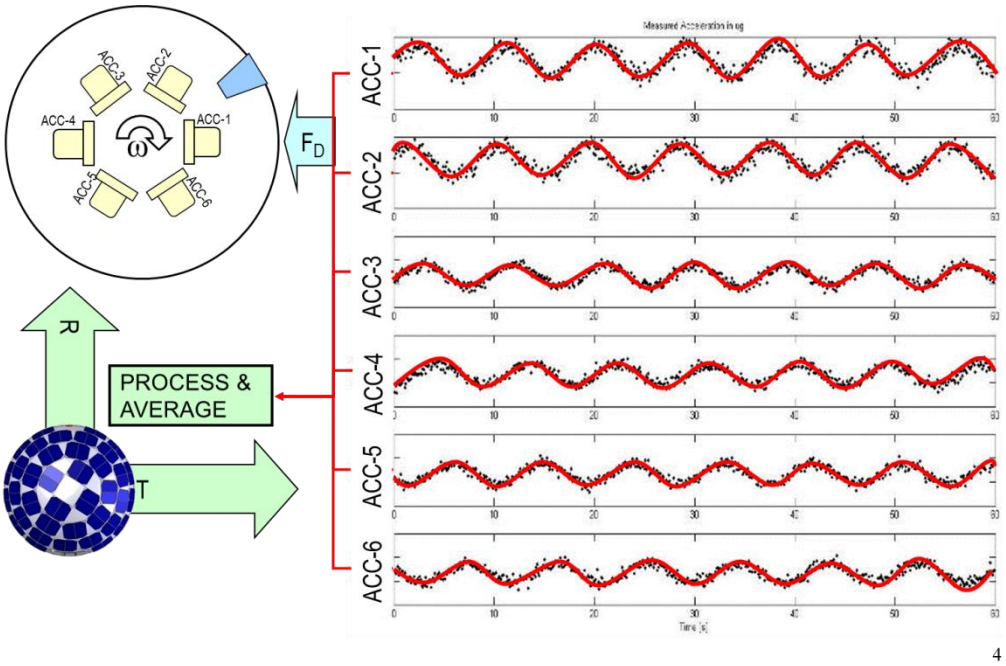

Figure 5 Predicted Accelerometer Output & Processing

Data Processing consists of performing a least squares fit to a sine wave function shown in Equation 2:

$$f(\vec{a}) = |\vec{a}|cos(\omega t + \phi) + \beta \qquad \text{Equation 2}$$

Here the amplitude of the sine wave is the acceleration as the sense axis of each accelerometer is scanned through the spacecraft velocity vector. The spacecraft rotation rate is represented in ω, the 60° phase shift of each accelerometer head is due to their hexagonal mounting pattern and is accounted for in the phase term φ, and finally the bias from parallel to anti-parallel measurement is seen in the form of ß which accounts for any DC offset. The accelerometers can only account for forces along the transvers and radial axes, this means that DANDE via accelerations alone cannot solely measure the cross-track winds with a component on the orbit normal axis hence the need for the WTS instrument to give insight into

this dynamic three dimensional environment. Further, cross-track forcing will likely be low in amplitude since the magnitude of the spacecraft velocity will be on the order of 7-8km/s whereas the wind vector magnitude along the cross-track axis will be more on the order of 500m/s. This 500m/s will vary based on the spacecraft position along the orbit as opposed to the constantly modulated input in the transvers axis making detection difficult beyond DC measurements.

2.3 Wind & Temperature Spectrometer Operations Overview

The WTS instrument is placed on DANDE to augment the acceleration measurements with correlated composition, kinetic temperature, and bulk velocity of the atmosphere in LEO. This is a very powerful measurement to take in conjunction with acceleration measurements since forcing on a spacecraft when sensed by itself does not describe major constituents and wind velocity.

This instrument was initially conceived as a method to sample the neutral thermosphere at Goddard Space Flight Center (GSFC) with Dr. Fred Herrero. GSFC began work with the DANDE program and in parallel began the development of a similar instrument in purpose and form factor called Winds-Ions-Neutral Composition Suite (WINCS). The extension of WINCS compared to the DANDE WTS is that it will sense the 3D wind vector in Local Vertical Local Horizontal (LVLH) while remaining oriented in the ram vector by having two orthogonally oriented WTS like energy spectrum scanning devices. Further the suite is comprised of a true time of flight mass spectrometer. This instrument collaboration with the University of Colorado has helped identify data collection techniques as

well as in kind donations of vacuum chamber facilities time to characterize the instrument. WINCS has become part of the NRL ANDE and University of Michigan CADRE missions. The former has already successfully launch, and the latter has been accepted into the NASA Educational Launch of Nanosatellites (ElaNa) cubesat launch initiative. DANDE will act as a complementary mission to these with the combination of WTS and acceleration data together on one platform.

This instrument will sense the neutral thermosphere as it does not have the ability to measure the ion species in the atmosphere. Internally the spacecraft will ionize the neutral particles and their kinetic energy can be determined through the use of a Small Deflection Energy Analyzer (SDEA) which is the same fundamental concept as the neutral particle detection on WINCS. The process by which WTS selects and detects the incoming species is described in sections 2.3.1-2.3.4. Graphically this is represented in Figure 6 showing the four discrete sections of the WTS.

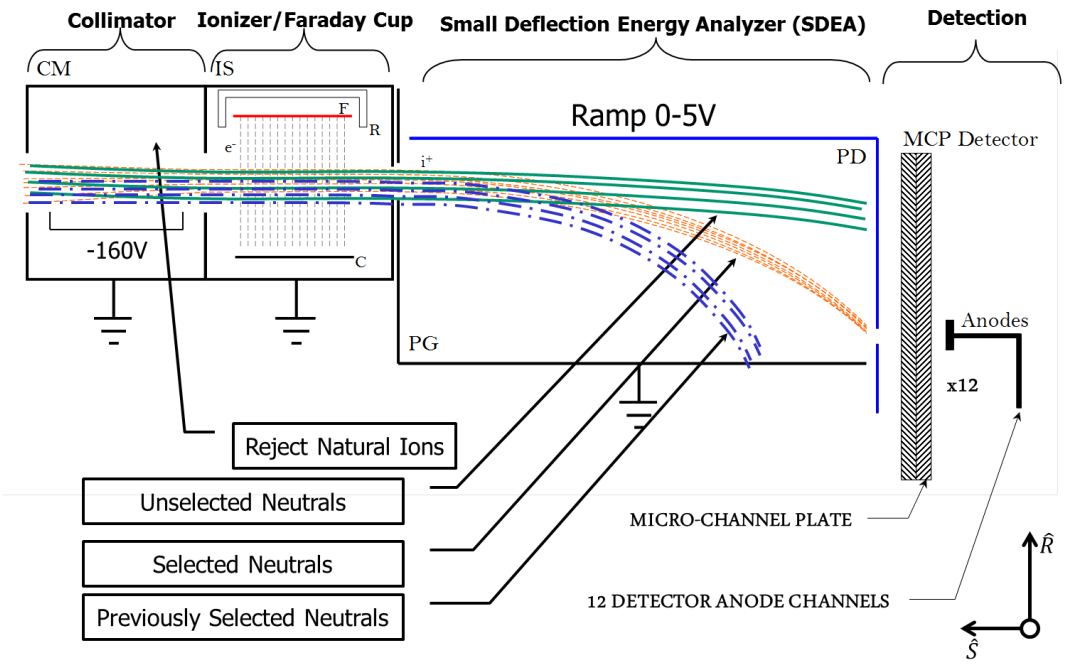

Figure 6 2D Cross-Section of WTS Internal Layout & Neutral Trajectories

2.3.1 Collimation

First, constituents of the atmosphere cross into the aperture of the instrument which is represented by a set of knife edge slits that collimates the flow to field of 3° vertical x 30° horizontal or a solid angle of approximately 0.03 sr. This first chamber serves a dual purpose as it has a plate internally biased by -160V to reject the naturally occurring charged particles in the atmosphere, this ensures that only neutrals will enter into the ionizer.

2.3.2 Neutral Species Ionization

Next is an ionizing chamber with an electron source running perpendicular to the flow through the instrument to ionize a small fraction of the neutrals, this is referred to as the ionization efficiency and is estimated at 0.1-0.01% of the total neutrals passing through this cross-section of the instrument [5].

2.3.3 Energy Selection

Considering then the ionized-neutrals entering the Small Deflection Energy Analyzer (SDEA) the primary function is to separate the particles in energy, which operates by creating a variable electric field. The kinetic energy of the particles can be described by $KE = \frac{1}{2}mV^2$, the largest contributor to the rise of the energy spectrum is the mass of particles since it is expected the variation in bulk velocity will be small. The bulk velocity is not directly the spacecraft orbital speed, this would be a unique case where no wind vector is present. Instead consider Figure 9 where the bulk velocity is the vector sum of the spacecraft and wind. There is a certain thermal variability, but this is captured in the spread of the energy peak, whereas energy selection is primarily focused on the peak energy.

2.3.4 Particle Detection

As the SDEA scans different particles trajectories are altered to varying degrees based on the electric field strength in the chamber. This is a form of kinetic energy variation resulting from mass, velocity, and charge. The forcing on the charged particles can for the moment be assumed to be uniform, however the momentum is not uniform which results in higher momentum particles requiring a larger electric field to bend to the exit aperture. Some portion of particles will exit the SDEA at any given moment which is defined as the point of energy selection. At the exit a micro-channel plate is positioned in the path and when the now ionized-neutrals impact the micro-channel plate a corresponding cascading shower of electrons is created which hits anodes on the backside, creating a current that can

be digitized into a count for science processing. The instrument will integrate at each energy level of the spectrum to collect counts. As designed the counting circuit can register 256 peaks/impacts/counts before rolling over and starting at a count of zero. This ambiguity has to be recognized in flight operations to avoid rollover at a peak anode, but not on the edges of the field of view. Figure 7 shows an approximated energy spectrum scan in a flight scenario.

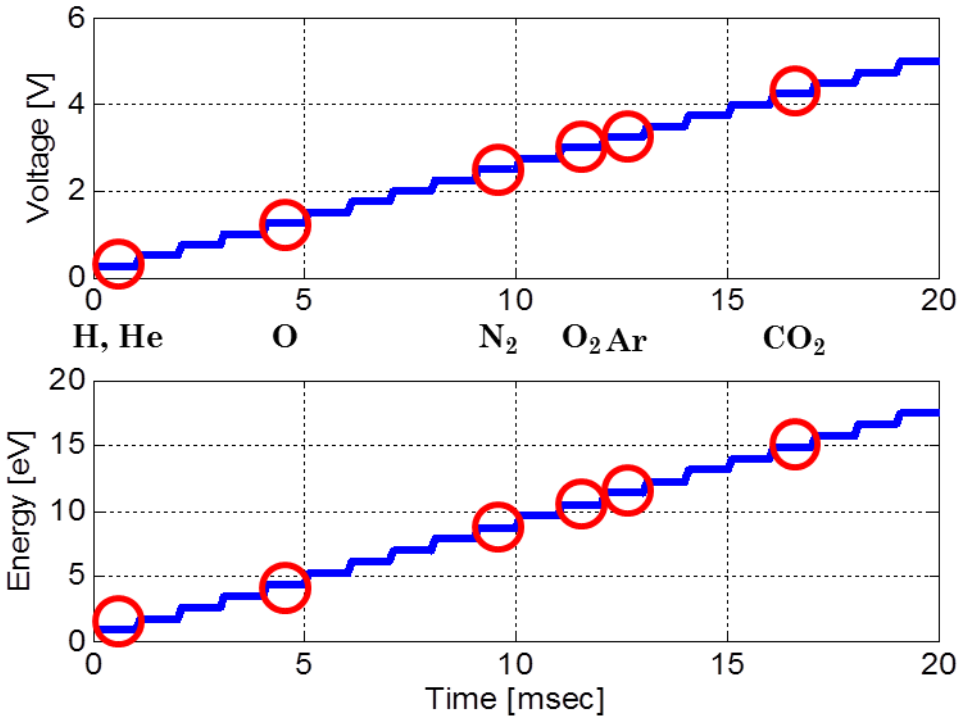

Figure 7 Energy Spectrum Scan

The scan itself is 20ms in duration with a 1ms integration time at each energy step. The top graph shows the voltage on the SDEA and is directly mapped to the SDEA plate factor conversion to energy in the lower graphic. The energy steps that register different species by the approximations of Table 1, which will be discussed shortly.

2.3.5 Measurement Design Constraints

Neutrals in Figure 6 are represented in three types those that are selected (dash-orange), unselected (solid-teal), and previously selected (dash-blue). Naturally occurring ions are shown in the collimator as being deflected out of the instrument boresight via the -160V repeller. Since the SDEA is designed to scan across a range of 0-5V the electric field inside the volume will vary in strength, the difference in the illustrated trajectories is then a function of the kinetic energy of the particles. The force acting on ionized-particles at any given electric field strength is described in Equation 3. The "previously selected neutrals" are those particles which have a low enough kinetic energy to be deflected into the bottom of the SDEA chamber. At the opposite end higher energy particles (those that are as yet "unselected") have little deflection in the electric field. This incremental scanning of the electric field is what provides a determination of the distribution of neutrals across a range of energies.

Considering then that the WTS does not utilize an acceleration stage in its design the kinetic energy is bound by a term for mass and velocity, shown in Equation 6. For the altitudes of the DANDE orbit the dominant particles are H, He, O, N_2, O_2, CO_2, and Ar from Figure 8, He, O, N_2, O_2, and Ar are plotted as a function of number density versus altitude using the NRLMSIS2000 model. To produce a plot such as this a geomagnetic quiet period is examined at low latitude with a Kp of 2, Ap, of 7, and F10.7 value of 100.

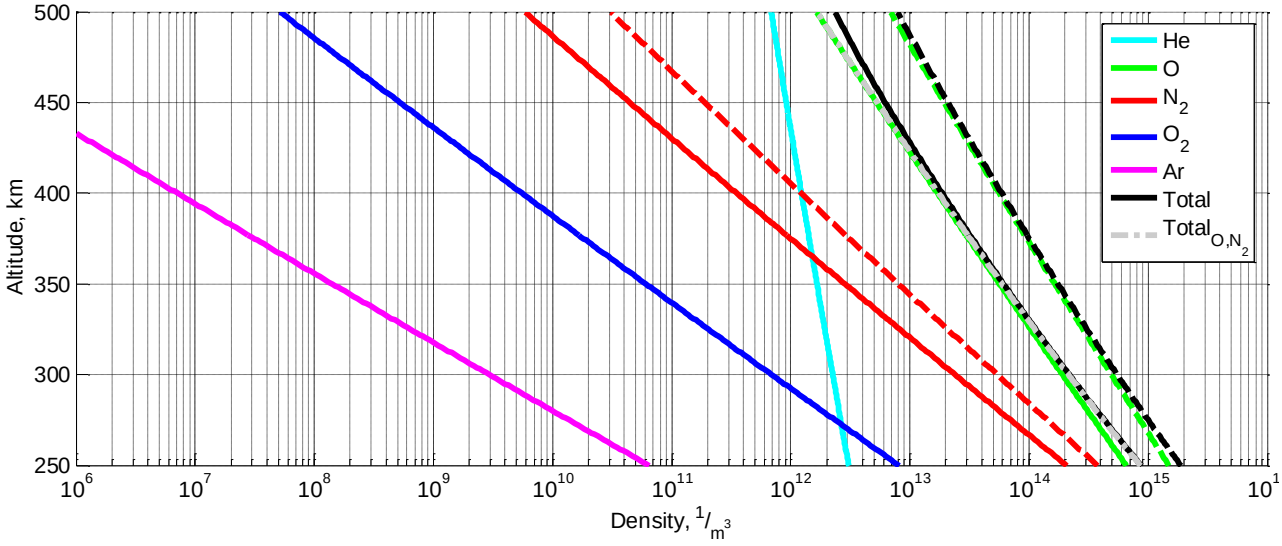

Figure 8 Atmospheric Composition between 250-500km

The main concern is what the predominant constituents are, here two totals are shown to make an argument that atomic oxygen and molecular nitrogen are of primary concern. The solid black line shows the number density of all molecules considered, and the dashed grey line is just the sum of O and N_2. From the lower bound 250km altitude up to 400km altitude the two track each other, at which point they diverge due to the continued presence of helium which drops at a diminished rate as a function of altitude because it has a larger scale height when compared against the number densities of N_2 or O_2 which are heavier species. This divergence is largely affected by the scale height of the species present in this rarefied atmosphere. However, that discrepancy is relative since this is a comparison of number density, consider for a moment mass density, the sum of O and N_2 dominates over the entire altitude profile since they are the largest mass contributors. Perturbations in the atmosphere will likely manifest as bias' in

number density as opposed to shifts in specific constituents, in all this suggests that O and N_2 being the primary concerns for number and mass density in a quiet condition would translate to the same behavior during an active period. This assumption works out seeing as the dashed green, red, and black lines represent the same model in a "active" period again at low latitude with Kp of 5, Ap of 15, and F10.7 equal to 200. By and large the increased activity exists as an increased number density of particles.

Since under quiet and storm conditions the primary species of the atmosphere remain the same, just with changes to overall number densities the primary constituents in terms of population can be asserted as O and N_2 in a region of interest ranging from 250-400km. The particles will differentiate themselves in the energy spectrum by their mass since their velocity with respect to the DANDE spacecraft is more or less uniform. As a rough order analysis of the spectrum to be sampled the particles will be accelerated to orbital velocities as DANDE moves through the atmosphere, these kinetic energies can then be described by Table 1.

Table 1 Estimated Energy Spectra Correlation to Particles

Particle	Mass [amu]	KE [ev}
Hydrogen, H	2	0.6
Helium, He	4	1.2
Atomic Oxygen, O	16	4.7
Molecular Nitrogen, N_2	28	8.2
Molecular Oxygen, O_2	32	9.3
Argon, Ar	36	10.5
Carbon Dioxide, CO_2	44	12.8

The kinetic energy of these particles can be found via $KE - \frac{1}{2}mV^2$ where m is the atmomic mass converted to kilograms (kg) 1.66 e-27kg/amu. Velocity in this case would be the uniform relative velocity of particles with respect to the spacecraft traveling at orbital speeds of 7-8km/s. KE can be converted from Joules (J) to electron-volts (eV) by the conversion of 1.60 e-19 J/eV. An electron-volt is a convenient unit for this study since 1eV describes the energy of an electron in a 1V potential. WTS is looking at more massive charged particles than an electron, but overall masses are small and it becomes unwieldy to use a unit of joules. This does not consider the effects of temperature variation of the species which will add a random distribution to these energies as well as the wind direction and magnitude.

Thermal effects of the atmosphere cannot be negated either as this will provide a distribution of energies to the same particle species. Neutral particles can be characterized as having upwards of 1000-1500K temperatures [2]. This thermal energy can be described as the product of the Boltzman Constant and the

temperature, $KE_{THM} = k_b T$ [3]Given the range of temperatures expected this would result in a range of 0.08-0.12eV around the primary energy peak. At the low end of the spectrum near atomic oxygen this would be ~2-3% of the bulk velocity contribution to kinetic energy. On the high end of the spectrum near molecular nitrogen this is ~1% of the bulk velocity contribution to energy.

Using Table 1 as a guide the DANDE system with the WTS will only need to sense up to 13eV to measure the major constituents with primary emphasis on O and N_2. These energies will change as a function of the scenario under which DANDE is sensing since any additive wind components along the spacecraft velocity vector will appear to increase/decrease the peak energy; this concept is illustrated in Figure 9.

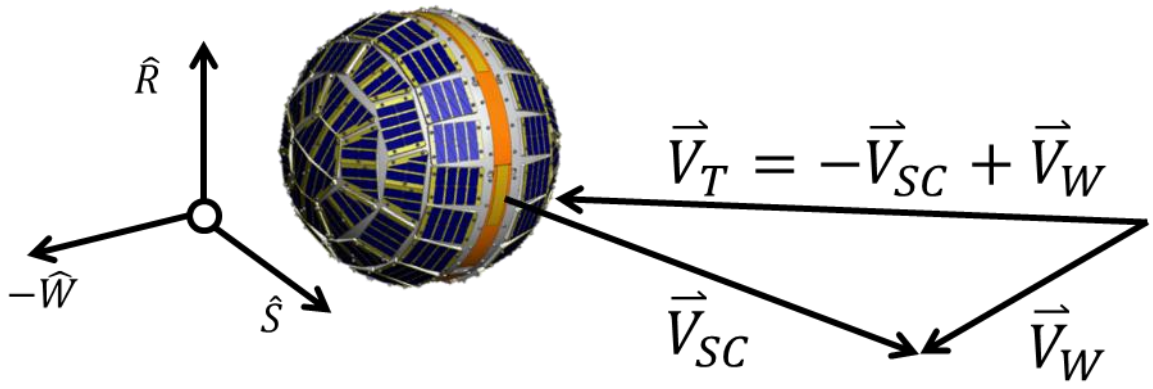

Figure 9 Wind Component of Velocity on the DANDE Spacecraft

In this image the spacecraft velocity vector is projected as $\vec{V}_{SC}$, in terms of the particles traveling into the WTS the negative of $\vec{V}_{SC}$ is calculated in $\vec{V}_T$. Removing the ambiguity of energy spectra change due to shifts in wind is a key concern and is partly resolved by geometrically sampling the cross-track axis shown in Figure 10.

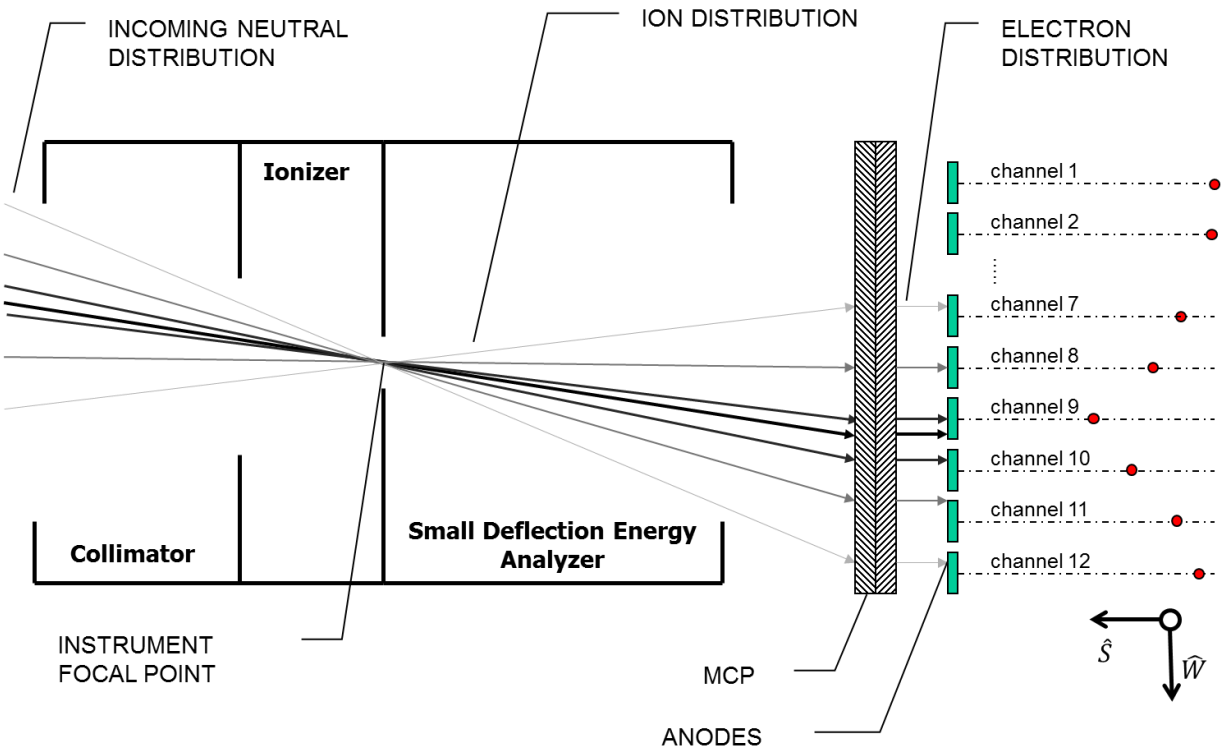

Figure 10 WTS Angular Sensitivity

Figure 10 is a horizontal cross-section of WTS (eg a top down look at the instrument). The aperture (left) allows a 30° field of view in the cross-track direction. In the figure a distribution of particles representing the wind vector is drawn entering the instrument and the location of the impact on the micro-channel plate relates to the count that would be picked up on the anode immediately behind that position. In the case of DANDE that 30° field of view is broken up into 12 anodes each representing about 2° resolution of the total velocity angle made with the spacecraft. This does not resolve whether the wind vector is constructively acting with the spacecraft velocity or not. This can be made observable by two independent means of verification. One method is to leverage tracking data being used to help fit the magnitude of the velocity for the spacecraft effectively removing

it from the energy spectrum and leaving just the wind magnitude. The alternative, as the satellite is spins about orbit normal the aperture of the spacecraft will face opposite the direction of travel, resolving the change in the energy peak between facing in the ram direction and then opposite would aid in determining the direction of the wind vector. Take for instance the case where the magnitude of the wind vector is largely opposed the direction of the spacecraft travel, as would be the case in Figure 9. When facing into the ram vector the total relative velocity magnitude would appear to increase in energy due to the total velocity magnitude being greater than the spacecraft velocity. As the satellite rotates 180° the total relative velocity magnitude would become less than the spacecraft velocity observed as a decrease in peak energies on the energy spectrum.

2.3.6 WTS Data Products

Directly from the WTS instrument the SDEA will scan the energy spectrum and the recorded counts will be downlinked to the ground at each energy step, this would result in a contour plot showing the relationship of energy, cross-track spread, and total counts, graphically this would result in something like the scenario of Figure 11. From this the first cut through the data a determination of the wind angle, neutral temperature, and wind magnitude can be derived. Wind angle is geometrically determined based on the 12 anode resolution behind the micro-channel plate. Temperature of the neutrals can be by observing the energy spectrum spread at the full-width at half max, that is to say, if the wind magnitude is defined by the energy of the particles at the peak number of counts, what is the overall energy spread at half of the maximum counts.

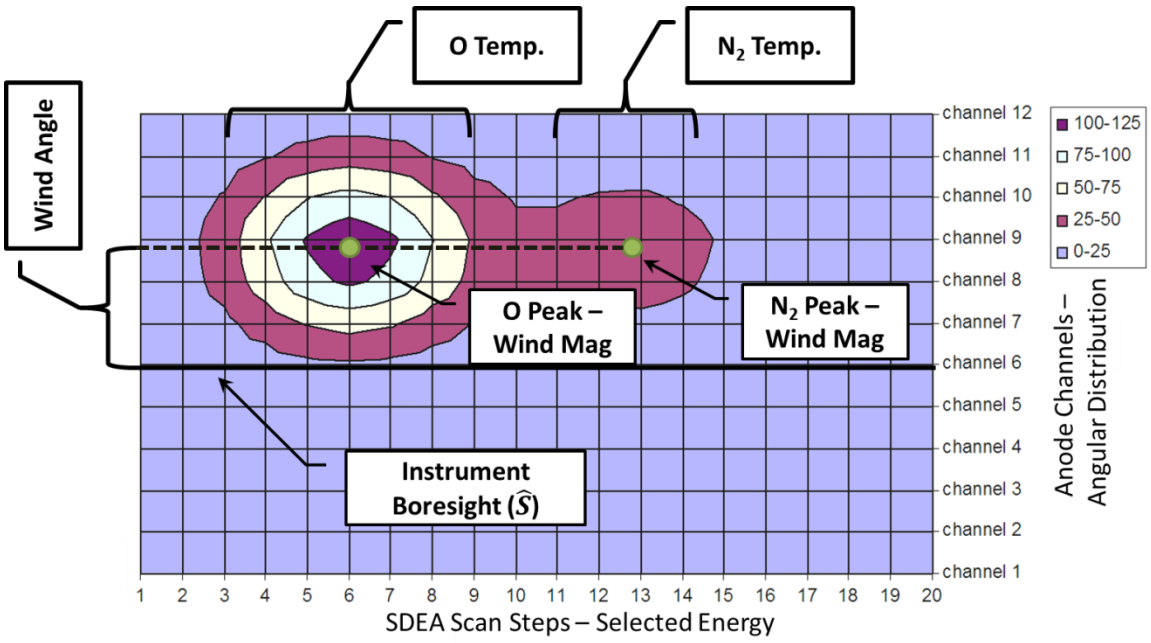

Figure 11 DANDE WTS Anticipated Data Products

The horizontal axis in Figure 11 shows the energy spectrum steps, not strictly locked to an energy, just a representative step in the scan. By calling out an O and N_2 peak one can assume these energies at step 6 and 13 are near 4eV and 9eV respectively. The vertical axis depicts the 12 channels of the WTS with the boresight defined on the middle of the channels. Each of the level 1 data products are called out on the graphic. Sensitivity of the wind magnitude comes from the statistical distribution of the species on the energy axis and is largely a function of the total number of observable counts. The atmospheric constituents can be represented as a Maxwellian distribution [2] and with that in hand based on the total number of counted particles at the peak error terms in a perfect system can be identified when sampling the neutral species, Table 2 [2] shows this breakdown.

These are tabulated considering a modest wind magnitude of just 10m/s, when substantially higher wind speeds may occur.

Table 2 WTS Peak Counts Error Break Down for 10m/s wind magnitude

Peak Counts	Percent Error			
	Wind Velocity	Temperature	N_O Density	N_{N2} Density
100	43%	1.3%	1.9%	1.3%
1 000	13%	0.4%	0.5%	0.4%
10 000	4.5%	0.2%	0.2%	0.1%

With the DANDE system there will be resolution limitations that will incur more observed error than this perfect setup, but this does provide a concept of the three figures of merit that must be considered in the development of the instrument and the modeled system. First the precision of the energy selection which will be the relation of the SDEA voltage to the selected energy, or the SDEA plate factor. The energy resolution, an expression of the energy width deviation as a function of the observed energy relates to the temperature sensitivity of the instrument. These two are used for fitting to the Maxwellian distribution of incoming particles to find a resultant wind vector. The wind vector is predicated on the overall number of counts that can be observed which is a function of the ionization efficiency as well as the transmission efficiency of the instrument suggesting that a proportion of the total ionized-neutrals entering for energy selection to the total counts on the MCP becomes a dominant consideration for flight operations. DANDE as a spin stabilized spacecraft will as it scans and integrates counts will be sampling over a finite angular segment of the of the sky so integration cannot be allowed to continue

indefinitely since there is information associated with the orientation of the spacecraft.

CHAPTER 3: EMPIRICAL WTS TESTING

During the course of development on the DANDE program there were three major campaigns of testing on the WTS unit, two of which occurred at GSFC and one using donated vacuum chamber facilities in Colorado. The GSFC testing opportunities were more centrally focused on the understanding of the ion optics whereas testing conducted in Colorado was focused on integrated unit testing and final checkout for flight operations. This focus on ion optics can be leveraged as truth comparison for SIMION modeling. Of primary concern are the energy selection, known as the SDEA Plate Factor, energy resolution, and the total transmission of ionized species through the instrument. All relate to the ability of the instrument to sense the atmosphere and the value returned to the ground, graphically the data products available are illustrated in Figure 11.

Analyzing the empirical data for the SDEA Plate factor will be a judge of the SIMION system ability to mimic the peak energy or wind magnitude of the primary constituents. Energy resolution will provide an understanding of the minimum temperature variation the instrument can detect due to the limitations of the ion optics.

Ion transmission speaks to the overall number of counts expected for observation to retrieve these other physical parameters, fundamentally more counts would achieve a higher signal. For this work transmission through the SDEA is the item of concern, the other major source of total achievable counts comes from the ionizer which has a reported efficiency of 0.1%. More neutral counts can be achieved

by one of two means, a higher transmission function, or integrating at the peak energy for a longer period of time. The former variable with respect to the DANDE system is not a viable option since at the time of writing the spacecraft is undergoing full system environmental testing and modifications are unfeasible. These simulations then have the ability to provide operational insights into how long the instrument must integrate for to achieve sufficient counts. Direct knowledge of the SDEA transmission of ionized-neutrals is not observable through test, it has to be inferred through the overall number of counts observed and the efficiency of producing ions from the external source in the chamber.

Historical data sets are examined here for the primary performance metrics of energy selection and resolution. Transmission proportion is not a metric that can be directly tested, however if confidence can be built between the physical system and the simulation of SIMION then simulations could provide insight to how efficiently ions are transmitted through the SDEA.

3.1 Testing Setup

The general philosophy behind testing the WTS is to ionize and accelerate remaining species in the vacuum into the entrance aperture of the instrument and run it under orbit scenarios for integration times. The key functional difference is the WTS is designed for sensing neutrals as opposed to naturally occurring ions because of charge discrepancies in the spacecraft and ionosphere. However, operational testing of the instrument with ions is a viable technique since the assumption can be made that ionizing the remaining neutrals externally will only

result in singly ionized species. This assumption is based off of the required energy to doubly ionize a particle like atomic oxygen or molecular nitrogen and maintain its mean free path, this is likely a low probability and contributes little to the overall signal read by the instrument. Functionally the instrument needs to deviate from flight operations since the ion repeller in the first section of the collimator will have to be turned off for this characterization study since if left biased there will be no bulk movement of neutrals at orbital velocities through the instrument.

The external ionizer consists of primarily five individual pieces that help to generate a flow of ionized particles into the instrument entrance aperture. Much like the instrument itself a filament and filament/electron repeller are mounted such that a stream of electrons run perpendicular to the boresight of the instrument. This electron beam will interact with a small fraction of the neutral species ionizing them. The void in which they are ionized is positioned between two plates that can have variable potentials with respect to the ground housing around the system. Aptly named the pusher and puller plates an electric field can be generated between the two accelerating now ionized-neutrals down the boresight of the instrument and into the entrance aperture. Generally speaking these plates were kept within a close enough potential so as to create a one volt electric field with a positive bias from chassis ground. Figure 12 depicts graphically the arrangement of the external ionizer with an actual image from testing to the right. Also shown is an extractor plate, in practice this was generally grounded instead of

run at a potential bias below ground due to fear that it was affecting the field free regions of the instrument itself.

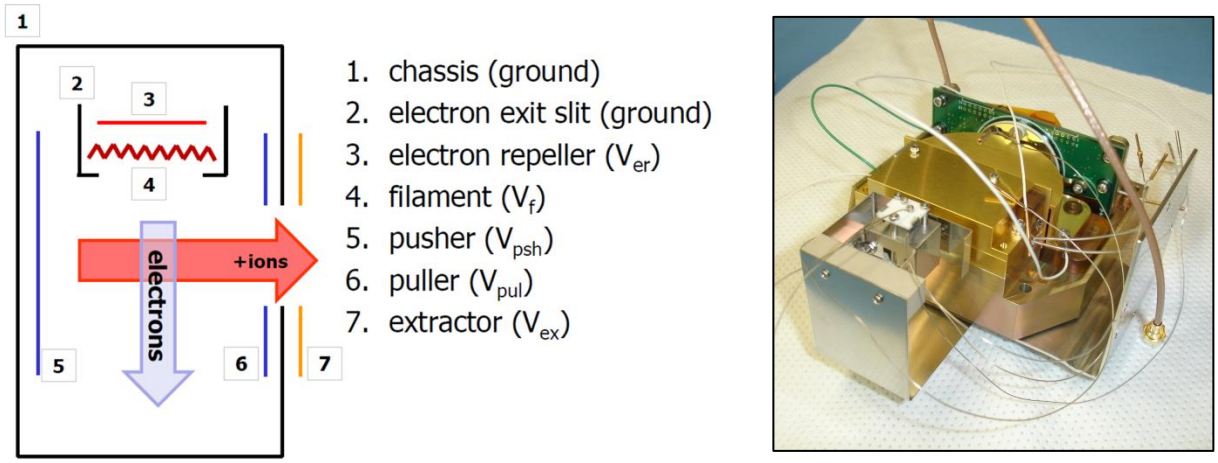

Figure 12 External Ionizer Diagram

Using this setup the incoming energy of the species is most simply approximated by the average voltage of the pusher and puller plates. Keeping the potential between the plates reasonably close together in theory helps to create a more uniform energy distribution into the instrument for sampling, however this field needs to be strong enough to fully accelerate ionized particles into the instrument. Preliminary testing results with this sort of a test setup show how the peak formed across the energy spectrum as the SDEA is scanned to higher voltages (higher energies) in Figure 13.

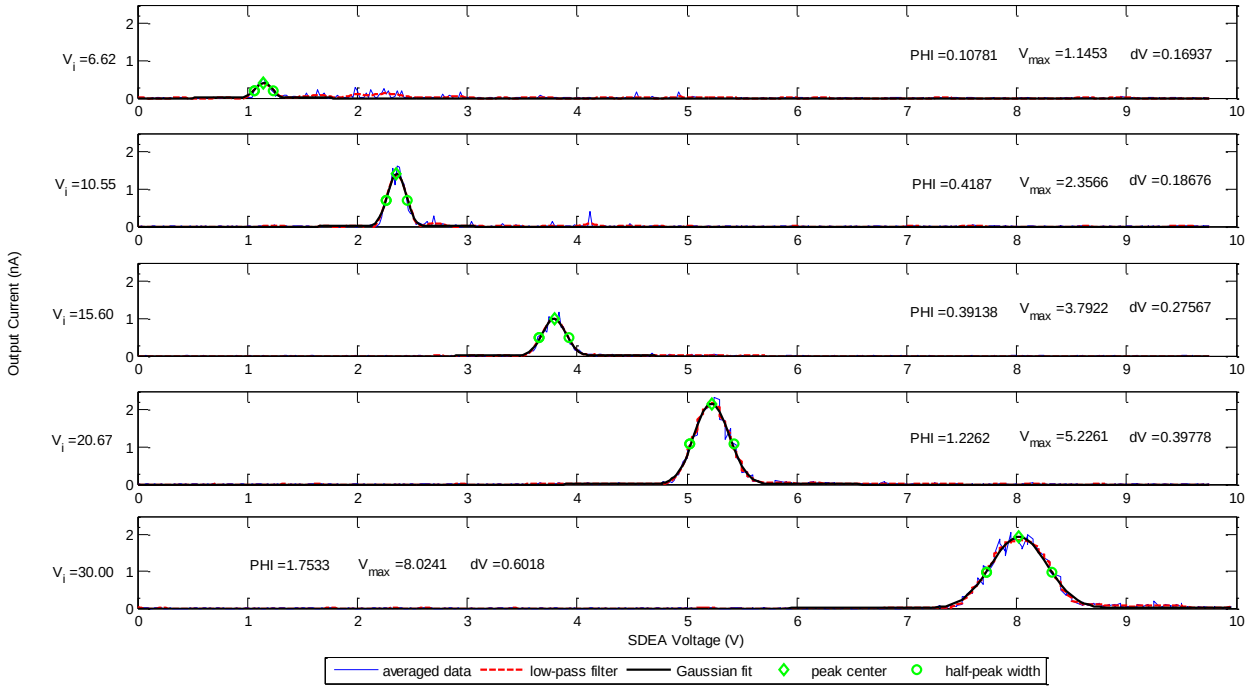

Figure 13 WTS Preliminary Testing at Goddard Spaceflight Center 2008

This data set is not representative of a final flight collection scenario since current was being sampled from a continuum as opposed to observing spikes in voltage on a comparator circuit. For these purposes though the accelerated ions are observed across a range of energies. Notice that in the different cases the energy is referenced with respect to the ionizer potential and the SDEA is being scanned to almost 10V when the final design only ramps to ~4V which is all that is required. This is due to the proto-type level testing being depicted as the SDEA plate factor discussed in the next section had yet to be determined and the required voltage to observe the naturally occurring ions was unknown.

3.2 SDEA Plate Factor

The aptly named SDEA Plate Factor relates the voltage potential on the deflector to the energy of the selected ion species. The physical process in play

behind energy selection is that DANDE takes advantage of the orbital velocities it achieves to separate atmospheric constituents in energy since they have differing masses. Atomic Oxygen then has about half of the mass of molecular Nitrogen so it peaks at about half the energy, recall the summary of constituents in Table 1.

Under normal operations DANDE WTS will scan the energy spectrum in discrete steps from 0V up to 4V, the forcing of the charged particles through this cavity is discussed in chapter 5 for the simplified test case of a parallel plate capacitor. Based on the design of the unit 20 discrete steps can be made over that voltage range, through testing an external voltage source was fed in for the SDEA bias in 2008 to first characterize for the SDEA plate factor prior to hard limits being placed on the system design. An advantage of simulation with SIMION is that a single uniform energy of ions can be flown into the instrument whereas during testing of the physical unit there are limitations to this uniformity. Recall the testing setup had an external ionizer that would take advantage of the remaining atmosphere in the vacuum by ionizing and accelerating them into the instrument through electrostatic fields. This process will yield a non-uniform energy distribution, but will peak in energy at approximately the average of the absolute ionizer and extractor plate potential on the ion source. Figure 14 describes this series of testing with the SDEA voltage running on the vertical and the Ionizer potential on the horizontal. The slopes associated with the trend lines are representative of the SDEA Plate factor since they are describing the ionizer

potential and the SDEA voltage at peak counts, the assumed point of energy selection.

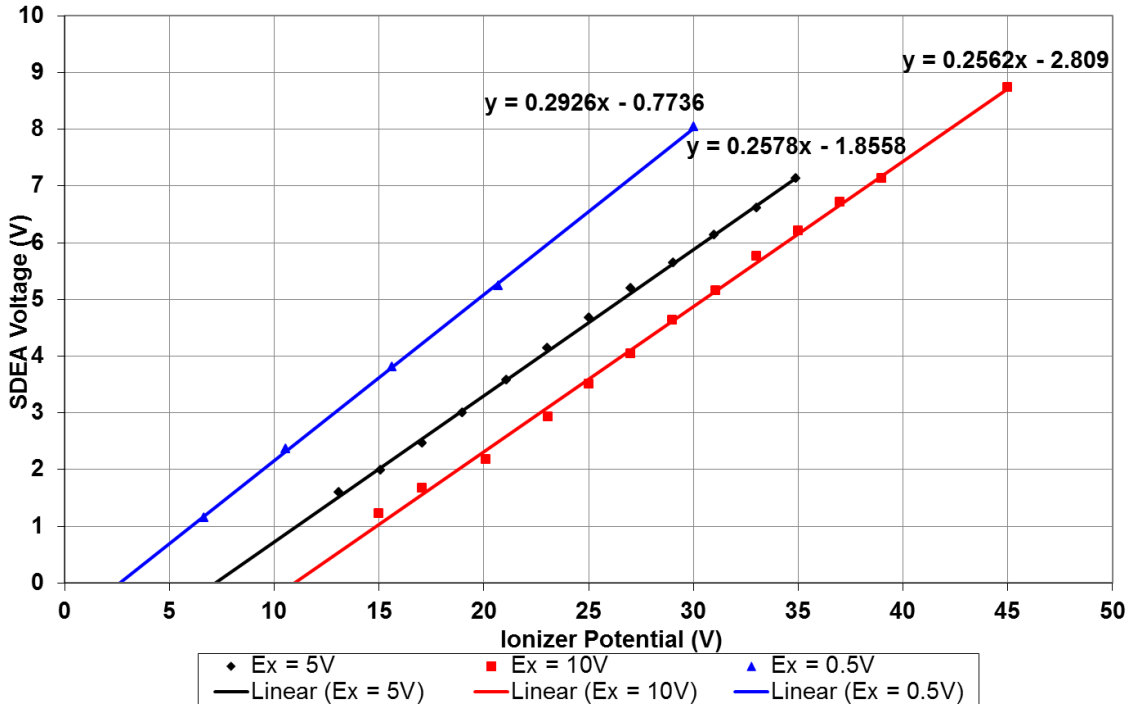

Figure 14 DANDE WTS SDEA Plate Factor Tests

Three different testing states are observed all relating to the distribution of ions accelerated into the instrument. Theory would suggest that the lowest number of counts but the most uniform distribution would be in a case of small differences between the ionizer and extractor, this would be the case of the test scenario in blue. The extractor is biased 0.5V below the ionizer making the ionizer potential just about the assumed peak energy; this conversion is taken into account with Figure 15. The averaged plate factor between these series of tests is 3.7eV/V, however there appears to be a strong dependence on the extractor voltage, the prevailing thought is that as the strength of the extractor increases the field is

permeating into the instrument and the true plate factor is much more likely to be in the range of the 3.4-3.6eV/V range where extractor voltage is lowest.

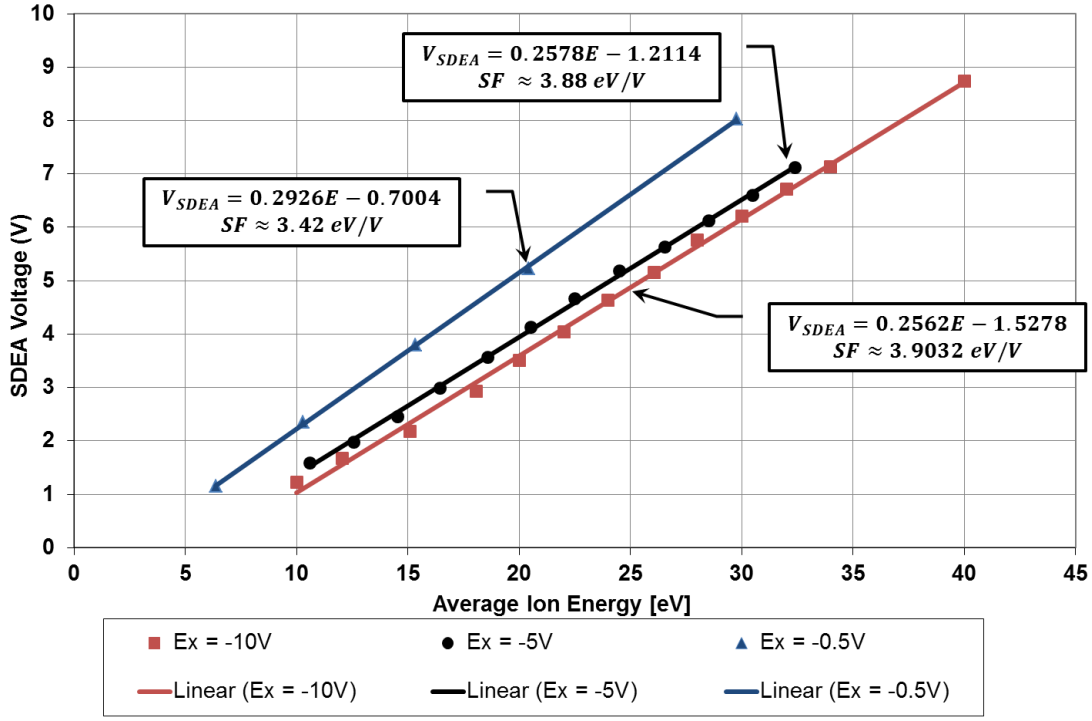

Figure 15 DANDE WTS Tested SDEA Plate Factor

These testing results can act as the truth measurements for the SDEA system when considering the response of a modeled system in SIMION. Ideally the SDEA plate factor in SIMION will fall into a range of 3.4-3.7eV/V using a uniform energy ion set and removing any additional fields from permeating into the instrument.

3.3 Energy Resolution

Where the SDEA plate factor maps to the data product for overall wind magnitude, energy resolution maps to the ability of the instrument to discern the temperature of the atmospheric species. Again testing from GSFC in 2008 can be leveraged. When the SDEA is scanned the voltage is noted, and through the plate

factor maps to an energy, by sweeping through the full energy spectrum an idea of how the instrument observes the rising and falling edges of the ion energies can be found. There are two physical limitations of the instrument to sense in the energy spectrum. The physical mechanism for selection is that vertical distance on the back wall of the SDEA represents the energy plane. While the exit aperture is only 0.013" that distance maps to a quantized range of energies, more over it fluctuates as a function of the selected energy at the time. The second issue in play is the finite distance of the entrance aperture, and the need to focus the beam of ions. In a perfect world the system would be in harmony if the forcing of the SDEA Plate factor altered the diameter of the ion beam from the entrance aperture 0.040" down to the exit slit 0.013". These two limits manifest as a ion energy being sampled across multiple SDEA voltages as opposed to a singular instant in time. Particularly due to the exit slit geometry the range of SDEA voltages that selects a particular energy ion species becomes wider with energy increase. The most efficient method to describe this is the energy width at half the peak counts or Full-Width-Half-Max (FWHM) and can then be described as a unitless scalar value.

From testing of the physical instrument the same series of extractor and ionizer potentials can be used, but as was described with the SDEA plate factor the conversion to the energy spectrum must be considered, Figure 16 takes this conversion into account from GSFC 2008 testing. Note that there are two trends present within all series of tests. First a linearly decreasing resolution as energy increase and then an asymptotic flat regime as energy again increases. Since the

source of ions is producing them in a continuum versus a singular set the linear decreasing trend describes a situation the energy width of the beam is wider than the energy resolution due to the ion optics. The turning point where the sampled beam is inherently narrow enough that the limiting factor becomes the ion optics is described by the asymptotic regime.

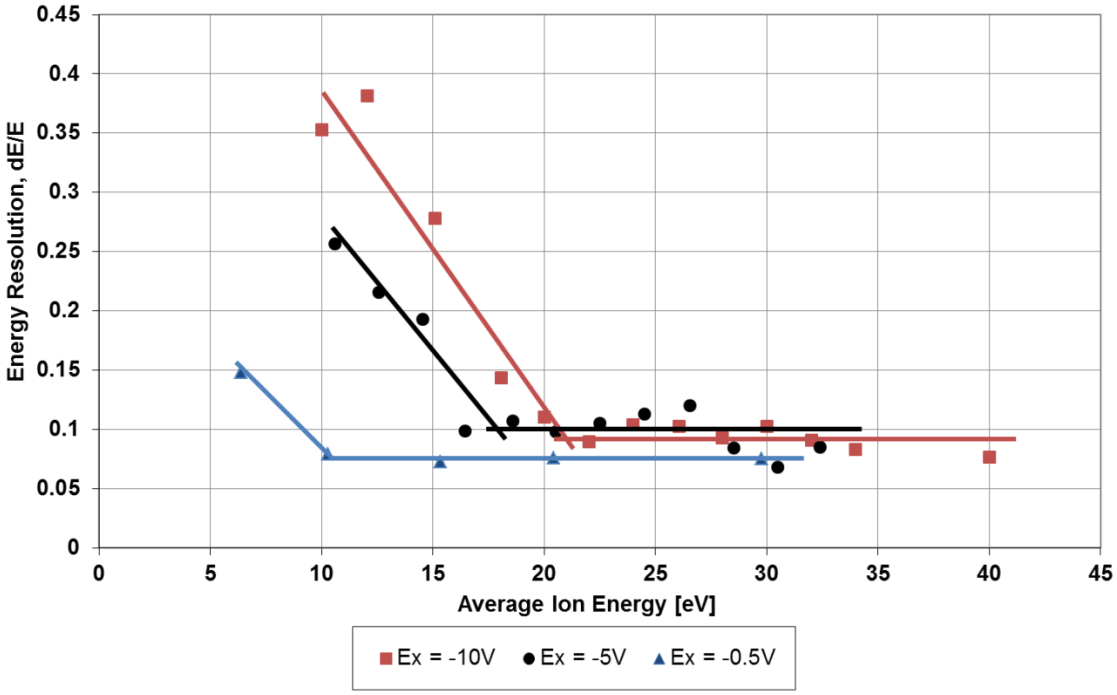

Figure 16 DANDE WTS Energy Resolution Testing

Previous statements of how narrow the beam energy is as a function of the extractor and ionizer potential difference a reinforced with this data since as the extractor potential bias is decreased the energy transition to asymptotic occurs at lower and lower energies. This can then act as a calibration of the ion source describing how wide of a energy beam is being created. Taking a step back to consider what the implications of the data are for a moment, as the SDEA is scanned in voltage when

the beam is uniform in energy there are instances where under a fine enough resolution scan the whole beam could in principle beam sampled multiple times. And based off of the observed behavior of the physical system this occurs when the beam energy width is less than 7-10% of the primary energy peak. SIMION should afford the opportunity to scan at much higher resolution with the SDEA using an impulse function energy by the virtue of flying only one energy of ions at a time with no associated distribution.

CHAPTER 4: SIMULATION SETUP

As was discussed with the physical unit testing setup it is prudent to discuss the test cases for SIMION in order to capture consistency between testing runs. Since 2D and 3D test cases are considered every effort is made to make them identical, however some deviances are identified and captured. Universally though only the SDEA is considered for test in SIMION since it is the primary driver of the performance metrics under consideration. This scoping of the test runs is beneficial because SIMION runs with a RAM resource limit of 2GB. Reducing the overall components being analyzed at any given time frees system resources for higher spatial resolution.

4.1 Two-Dimensional Workbench

Since the SDEA acts as the primary driver for the overall system performance there is a further benefit as an assumption of axial symmetry down the boresight can be made enabling a very simplified system for test. Chapter 5 will discuss the validation case for SIMION using a parallel plate capacitor, in essence the SDEA is a parallel plate capacitor with a variable electric field. A 2D simulation of the SDEA then acts as a good intermediary between the simplified SIMION evaluation case and the true 3D system. The profile of the SDEA is shown in the 2D simulation evaluation in Figure 18.

During buildup of the workbench a resolution of 0.1mm per grid unit was selected as the minimum spatial resolution for the potential surfaces of the SDEA. This resolution selection was not arbitrary as experimentation with the 3D cases

showed that with the SDEA as designed the resolution that was achievable without exceeding system resources for simulation was again at 0.1mm. While there are not nearly as many nodes in the 2D profile of the SDEA for the sake of consistency across platforms the value was held constant for the most limiting scenario. Features of the SDEA such as the knife edges on the entrance and exit apertures are maintained through simulation here as well as spatial separation between the SDEA deflector and ground as well as the micro-channel plate.

4.2 Three-Dimensional Workbench

SIMION has provisions in place to accept in stereo-lithography files (.STL) which can be directly imported from CAD software packages like Solidworks or AutoCAD. Files simply need to be named with a consistent convention and then individual parts can be imported and treated as different potential arrays which in test cases allows for different potentials to be applied to different parts as is the case with the true system [8]. It is as this import phase that the spatial resolution must be selected, and with the size of the SDEA only resolutions down to 0.1mm can be generated otherwise the number of nodes in the model and data resolution per node per axis exceeds the upper limit 2GB of system resources available to the simulation.

The added benefit to using the STL file and importing is that spatial geometries are maintained through the process and leverage the bolting locations from the CAD model as references as opposed to maintaining the spatial references

by hand. The final imported as built SDEA is shown in Figure 25 as part of the results evaluation for the 3D test cases.

In an effort to characterize the differences between the 2D results and 3D results several different geometries were explored that approximated the width of the SDEA as infinite in terms of the electric field structure in an attempt to make a 3D representation of the 2D profile, in these cases there were results that were tested in a resolution that was not at the 0.1mm spatial limit because of the addition of significantly more nodes to the scenario. This does not have a profound effect on the macro scale as ions fly across the chamber, but it does influence the small features such as the knife edges.

4.3 Ion Species Simulated

For each flight scenario in SIMION a single set of voltages can be applied to the potential arrays, after the simulation run the potential arrays can be changed. It is by this set, test, reset method that a quasi-continuous SDEA ramp can be achieved. For each voltage run 1000 ions were flown at a uniform energy and the Cartesian coordinates at the impact site were captured.

As the SDEA potential is ramped through the full dynamic range a uniform energy set of ions can be flown through the SDEA chamber. With SIMION an ion mass and velocity can be specified, or a mass and energy. Since these two concepts are intertwined the desire was to fly a uniform energy instead of a mass distribution. This would mean a single mass could be selected for all points in the SDEA ramp and the velocity of the particles would change as a result.

At the entrance aperture to the SDEA or alternatively the critical focal point of the instrument a uniform distribution of ions were flown with the same unit vector velocity directly into the SDEA. In the case of 2D simulation a line distribution was used where the ions under test were evenly distributed across the entire vertical entrance. For the 3D case a circular distribution was used, which mimics the line distribution of the 2D, but is revolved around the boresight axis so as to capture the round entrance aperture. The width of both distributions was such that the entrance aperture was filled instead of scenario where the bulk of the ions were in biased towards the center of the aperture. This distribution scheme was chosen since it would more accurately represent the diffuse external ion source, but also test the geometric limitations for the resolution of the system.

Uniform energy species are tested from the SDEA potential 10mV lower than the start of their selection band pass, across the band pass until 10mV greater potential than it takes to select any of the ions. Since 1000 ions are flown at each energy it would not be computationally efficient to fly several sets of energies with each test scenario instead after a scan across one energy is complete the next ion energy is cued up and the test sequence is repeated for the appropriate range of SDEA potentials.

CHAPTER 5: TWO-DIMENSIONAL TEST CASE

Work to determine the utility of the SIMION software tool kit for modeling ion optics at CU Boulder began with an independent study research assignment by James Binney over the 2010-11 academic year [1] The concept of the work is to show that an analytic model of a simple geometry matched up to the observed responses in a matching SIMION workbench. This thesis uses information gathered from that study to link empirical testing to observed model responses and then building more complex geometries of the detection scheme inside of NMS.

The test case used is an infinite parallel plate with a constant electric potential across the gap of the plates, graphically this is represented in Figure 17.

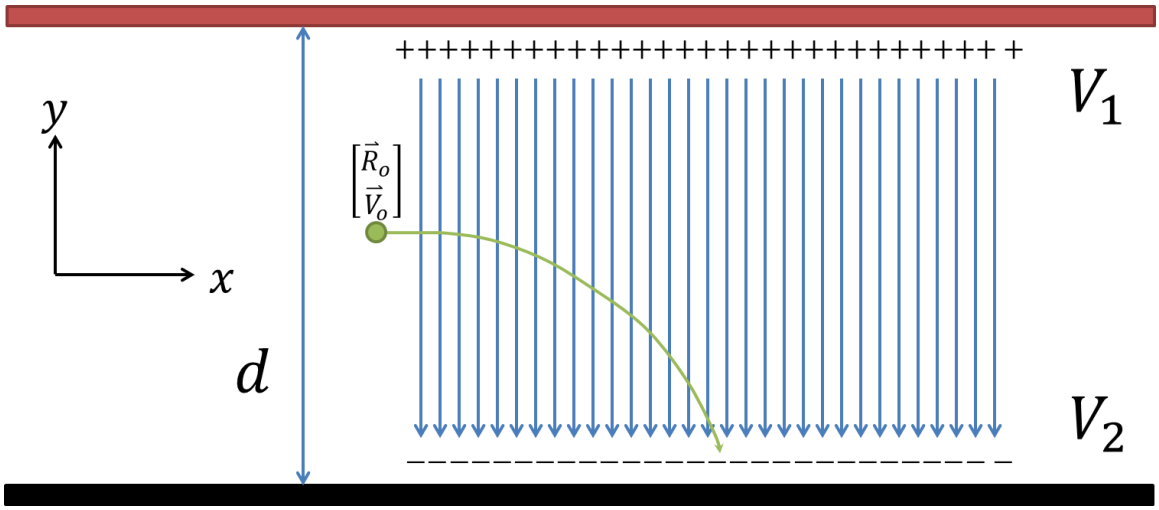

Figure 17 Infinite Parallel Plate Constant Electric Field

A particle with charge q shown in green is introduced with some initial position an velocity. As the particle enters the electric field a force is induced on the particle that can be described by Equation 3.

$$\vec{F} = m\vec{a} = q\vec{E} = q\frac{V}{d} \qquad \text{Equation 3}$$

The physical parameters of the particle are represented by the mass (m), and charge (q). Since this is a simplified case the force will only act in the y-axis of the diagram with the height of this gap being represented as d. Equation 3 can then be manipulated to describe the acceleration of the particle as shown in Equation 4.

$$\vec{a} = \begin{bmatrix} a_x \\ a_y \end{bmatrix} = \begin{bmatrix} 0 \\ \frac{qV}{md} \end{bmatrix} \quad \text{Equation 4}$$

This description of the acceleration can be numerically integrated to describe position as a function of time, however the fact that it is easily represented as a constant means a position can be analytically represented, shown with Equation 5.

$$\vec{R}(t) = \begin{bmatrix} R_x(t) \\ R_y(t) \end{bmatrix} = \begin{bmatrix} R_{x_o} + V_{x_o} t \\ R_{y_o} + V_{y_o} t + {}^1/_2\, a_y^2 t \end{bmatrix} \quad \text{Equation 5}$$

SIMION does not allow for a truly infinite setup in its workbench, however driving down a bit on the nature of the setup the desire is to have a uniform electric field for the particle to move through. In this case making a setup in SIMION is feasible, the particulars of setting up a workbench are described in further detail in CHAPTER 4: with regards to how two and three dimensional cases were built. The parameters for the test are outlined in Table 3 [1].

Table 3 Parallel Plate Physical Parameters

Parameter	Value	Unit
Particle (Atomic Oxygen: O^+)	16	amu
Kinetic Energy	1-7	eV
d	30	mm
V	5	V

The particle definition of using atomic oxygen constrains the mass, the only remaining item to consider is the velocity which in this case to test the deviation over a spectrum is swept between 1 and 7 electron-volts. Electron-volts are one mechanism for describing the kinetic energy of an object and the conversion to the more standard energy unit of a joule is $1.602\ 176 \times 10^{-19}\frac{J}{eV}$, with this conversion in mind the kinetic energy can be describe as shown in Equation 6.

$$KE = \frac{1}{2}mV^2 \qquad \text{Equation 6}$$

Solving for velocity and accounting for the conversion of Joules to Electron-Volts as well as AMU to kg is shown in Equation 7.

$$V = \sqrt{\frac{2KE_{eV} \times 1.602\ 176E-19\frac{J}{eV}}{m_{amu} \times 1.660\ 539E-27\frac{kg}{amu}}} \qquad \text{Equation 7}$$

Considering the range of energies this shows that the velocities under scrutiny are in the range of $3.5 - 9.2\frac{km}{s}$, since the discussions of this modeling are for a spaceborne instrument that range is fortuitous because it is representative of orbital velocities WTS will measure.

Suppose then the simulated particles for this test are given initially a pure velocity in the X-Axis and are centered in the gap between plates at a height of 15mm. Using SIMION and Equation 5 an assessment of the predicted impact points on the lower potential plate can be made, this is summarized in Table 4. A total of 20 ions were flown each varying in energy by 0.3eV to make the spread from 1eV up to 7eV.

Table 4 Parallel Plate Simulation Summary

Ion Energy [eV]	Analytical [mm]	SIMION [mm]	%Error
1	18.9727	18.9737	0.0053
2.5	25.7506	25.7519	0.0050
4	32.2800	32.2817	0.0053
5.5	37.6950	37.6969	0.0050
7	42.4243	42.4264	0.0049

Considering that both data sets are simulation the relevance of the deviations between each other of 0.005% does not represent a statistically relevant change. To that point since this was a back of the envelope comparison the variability of the ion trajectories which may be seen in SIMION as it predicts the flight path of particles has not be quantified since only one ion is analyzed at each energy level. With the analytical and SIMION models deviating by so little with respect to each other it lends credence to this software being used as a viable modeling tool. The next major step forward is to show how well simulated data matches to empirical data gathered through test.

CHAPTER 6: TWO-DIMENSIONAL SIMULATIONS

The simplest geometry of a SIMION simulation of the SDEA would be akin to the graphical representation in Figure 6. In using the 2D case the assumption is made that there is little influence of the finite dimensions of the SDEA in the cross-track or angular sensitivity to winds. This removes the possibility of analyzing for angular sensitivity, but still allows for furthering the understanding of the responses to SDEA voltage, referenced as the SDEA plate factor, and the energy resolution.

6.1 Validation of Geometry

There are limitations to the analysis of ion optics that SIMION can provide, namely a minimum resolution for the gridded system assembled. The program itself is limited to the use of only 2GB of RAM on the system performing the analysis. For the 2D geometry a 0.1mm (~0.004") node resolution was used and ideally maintained across 2D and 3D geometry variants. The as built system was manufactured with tolerances approaching 0.05mm (~0.002") for entrance and exist features to the SDEA, and for mounting 0.125mm (~0.005"). This limitation puts the simulated system in the realm of the tolerances although it would be desired if these could be much lower than the tolerances, but in the interest of maintaining a consistency across 2D to 3D simulations the 3D geometries require a significant increase in nodes that do approach the limitations of SIMION.

To preserve the properties of the SDEA the key dimensions to consider are the length (32.62mm, 1.285") and height (14.98mm, 0.590") of the SDEA, the distance of

the center of the entrance aperture to the deflector plate (0.76mm, 0.030") and similarly the exit aperture to the ground plate (0.76mm, 0.030"), then finally the aperture geometry as a knife edge within the restrictions of the simulation resolution with the same orifice diameter at the entrance (1.01mm, 0.040") and exit (0.33mm, 0.013"). These dimensions are shown in Figure 18 as well as the NMS Master Assembly [8] drawing provided by the DANDE program.

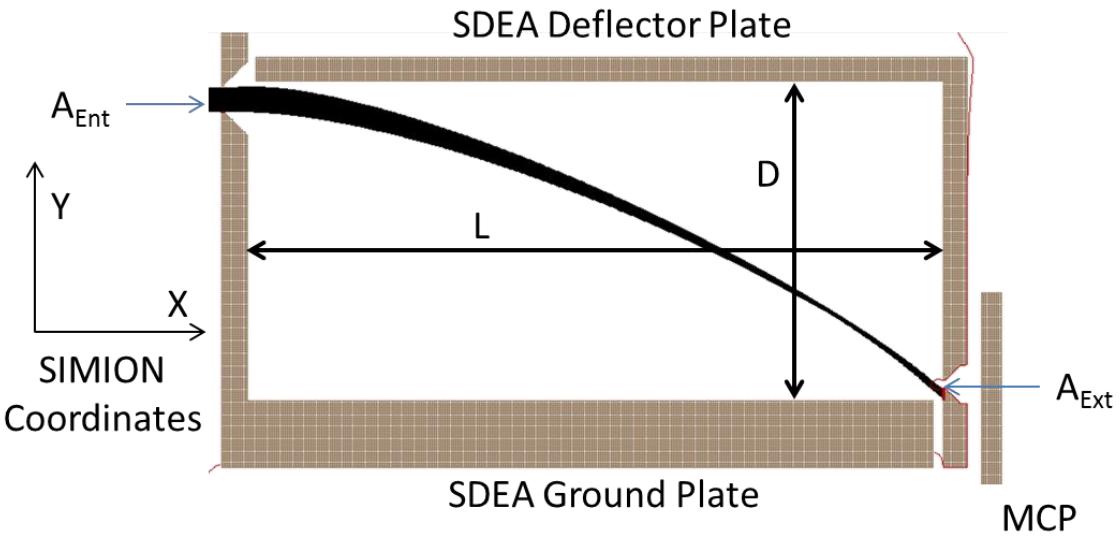

Figure 18 2D SDEA Geometry

The entrance and exit apertures are called out specifically, recall that the definition of these points is constrained by two separate features. Also for reference the coordinate system used in SIMION is shown, consider the DANDE coordinate system shown previously in Figure 9. The SIMION X-Axis in a horizontal state roughly maps to the along-track axis of the spacecraft and the Y-Axis would then map to the radial vector of the spacecraft. For the physical system then the cross-track would be into the page, but for 2D analysis is neglected. Note that the

trajectory of ions is depicted in this graphic, their path through the SDEA has been altered by a potential on the SDEA deflector plate to the point where they are impacting below the exit slit corresponding to scenario just past ion selection.

6.2 SDEA Plate Factor & Energy Resolution

Since a uniform energy set of ions (recall a total of 1000 per voltage step in the SDEA ramp) can be sent through SDEA discrete energy states can be tested, here a set of ions is flow at each 1eV increment from 1eV to 12eV ions with samples taken in SDEA 5mV increments. Figure 19 shows the total number of ions counted as impacting the SDEA when flown at each energy level.

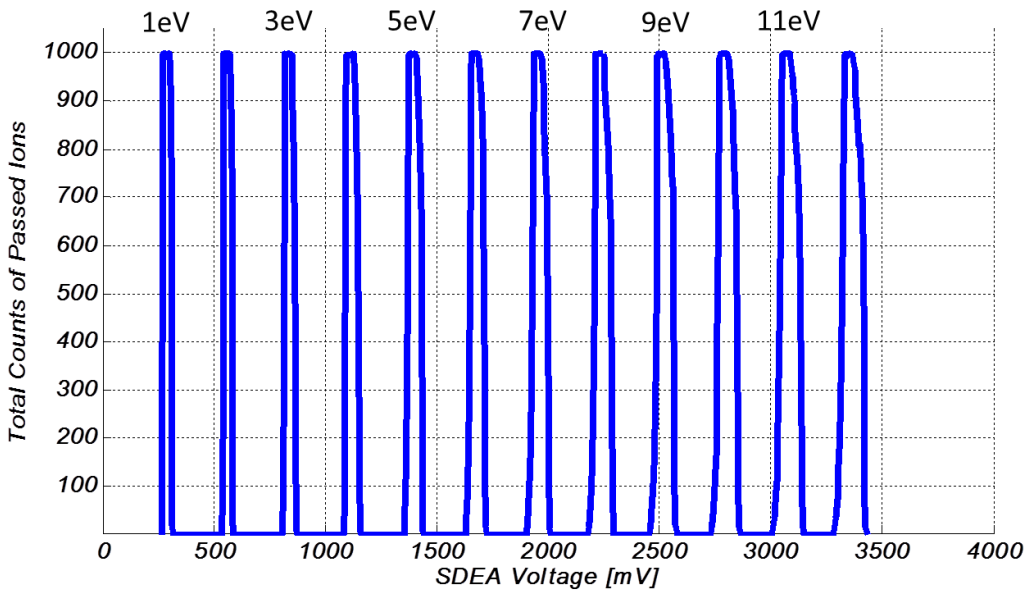

Figure 19 2D SDEA Ion Passage Profile

Notice that the selected energy region is not quite triangular in shape as predicted in the heuristic GSFC predicted results based on the length to height ratio of the DANDE SDEA. Also this graphic depicts total counts, and at the peak there is 100% passage. To find the SDEA Plate factor since no single peak exists an assumption

must be made that it lies in the middle of the selected energy region of 100% passage. The energy resolution defined off of the full width at half max is determined by fitting a cubic spline on the rising and falling edge of the selected energy region and evaluated for the SDEA voltage at 50% passage.

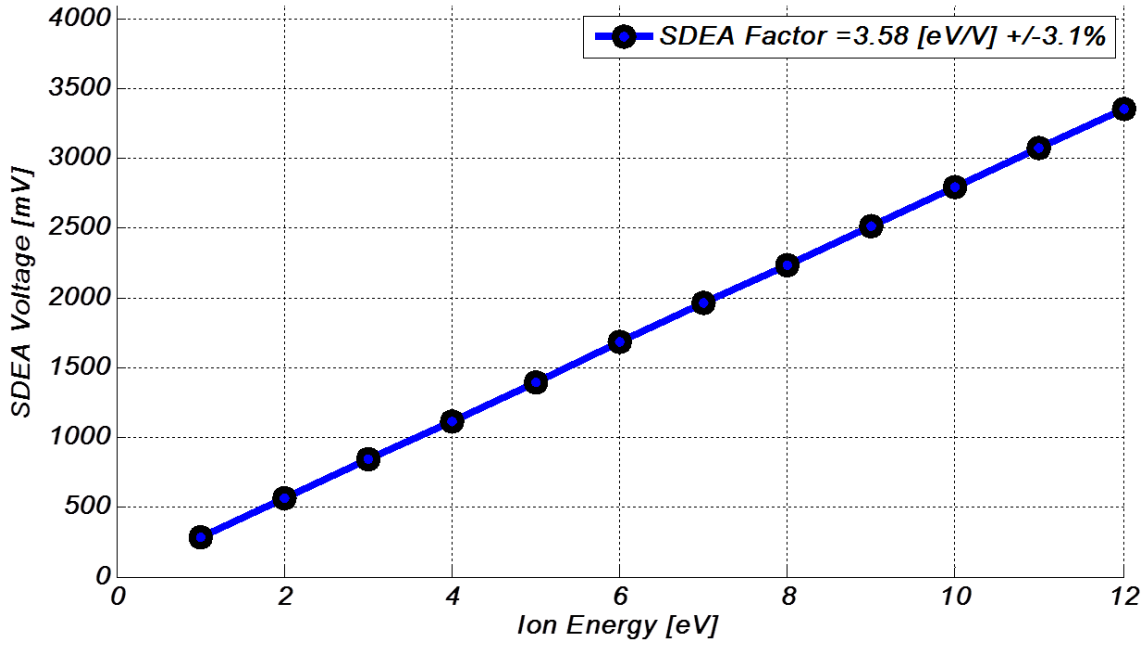

Figure 20 2D SDEA Plate Factor - As Built

Figure 20 shows the result of this analysis for the SDEA plat factor. The estimated value for energy selection is approximately 3.58eV/V which is sufficiently close to the empirical value of 3.6eV/V. The tolerance on that value is achieved by estimating the plate factor using all the lowest voltages in the selected energy region and decreasing the plate factor and then similarly using all the highest values to increase the plate factor. This first look suggests that a 2D simulation does map to the physical system built for DANDE, the other parameter of interest is energy resolution shown in Figure 21.

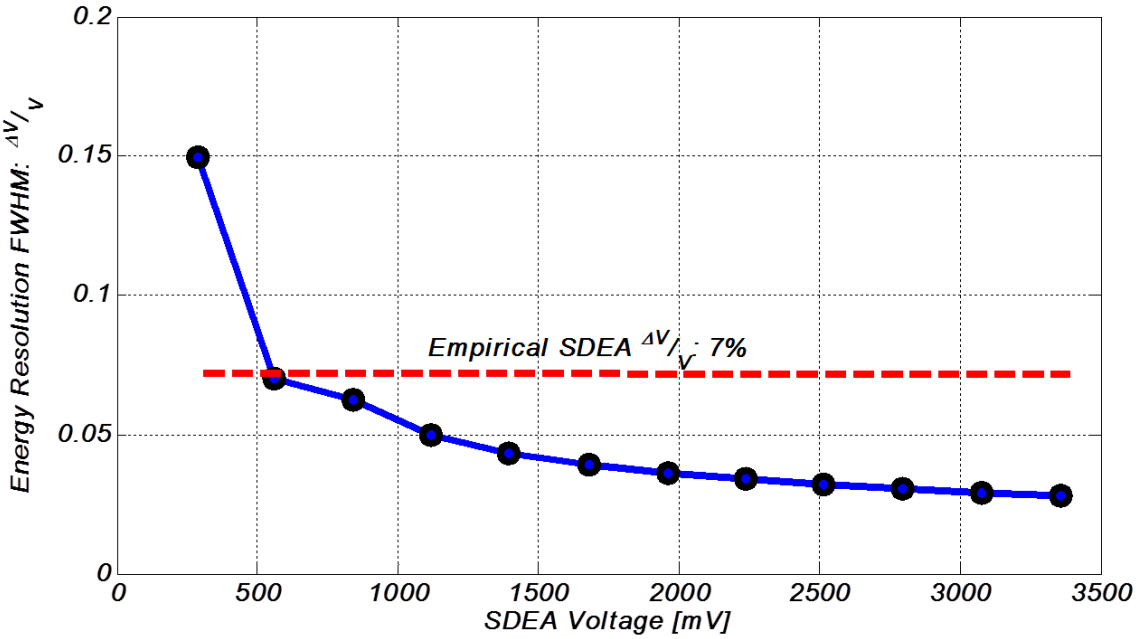

Figure 21 2D SDEA Energy Resolution

Interestingly the 2D SDEA performs with a much better energy resolution than the physical system. Recall that the concept of the Full-Width at Half Max would represent the region that would not be considered statistically relevant for the selected energy region. This would indicate that the range of selection voltages is much narrower than testing and ultimately the temperature and velocity measurement precision increases. However operationally the system in testing responded with a flat trend, as shown here the system has a non-linear trend to energy resolution, meaning that 4eV ion precision is fundamentally different from 9eV resolution. This has greater ramifications since it affects the concept of total counts used in O:N_2 ratio as well as the temperature measurements. The empirical testing did not get to benefit from a uniform ion input and since it was sampling

from a continuum of ion energies during test then it is conceivable the 7% empirical value was a limiting function of the external ion source not the SDEA.

These three pieces of information that form the basis of the investigation for the SDEA (Ion passage, SDEA plate factor, and energy resolution) will be investigated again, considering the SDEA Plate factor observed within the bounds of the empirical testing helps root this simulated system with the physical. Curiously and of concern the energy resolution appears to be a function of ion energy versus the empirical evidence suggesting independence. The high proportion of passed ions is also something calling into question the validity of the results observed.

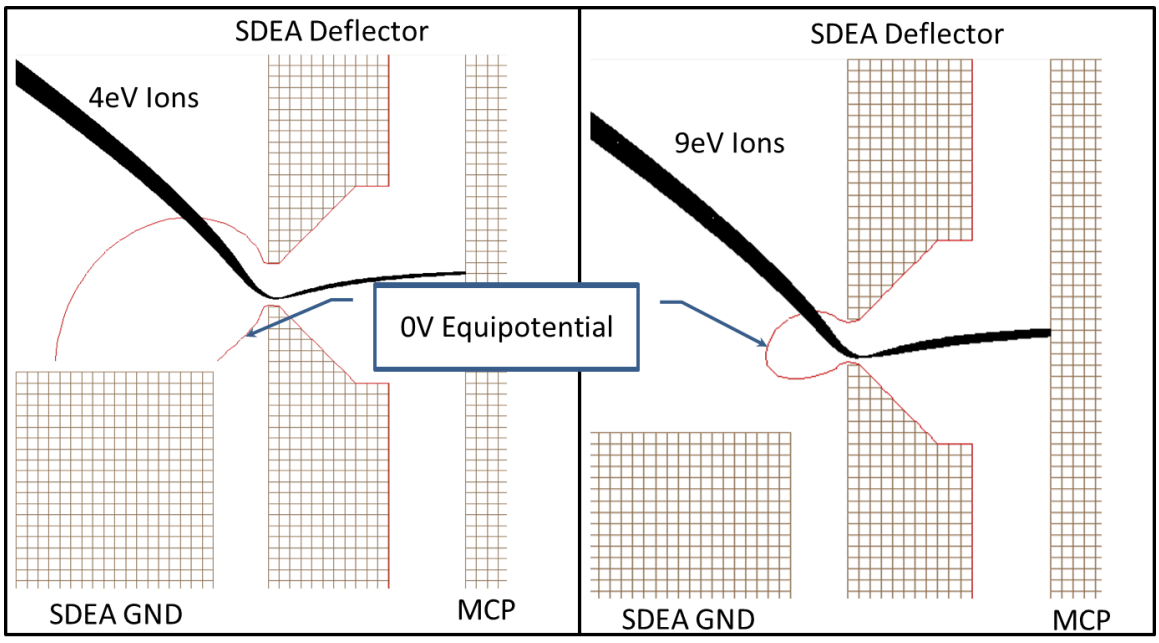

Figure 22 MCP Impact on SDEA Ion Selection

Figure 22 is taken from the graphical output of SIMION when 4eV ions (approx. O energy) and 9eV ions (approx. N_2 energy) are selected at their respective deflector

voltage. The micro-channel plate is represented with a bias off the SDEA ground plate of the operational system voltage of -2500V. In red a 0V equipotential is plotted around the exit aperture of the SDEA. This particular reference point is of interest since it represents the threshold between the SDEA being the dominant forcing mechanism on the charged particles and the MCP being dominant. Ideally the SDEA should not be dominant inside the SDEA chamber at all, if it is then ions entering the "bubble" influenced by the SDEA have a propensity to be selected because the electric field presented by the SDEA to MCP is extremely strong and biased to the MCP. This equipotential also appears to have a relationship to the selected energy, notice on the left the sphere of influence is much larger with the 4eV ions than the 9eV ions largely because the SDEA deflector voltage is lower for the selection of the 4eV ions. The result of this influence would most likely manifest itself as an increased bandwidth of SDEA voltages that low energy ions would be selected over disproportionate to the resolution of the ion optics. To that end because this is a function of SDEA voltage the energy resolution response would behave in a decaying exponential function which is observed in this series of test.

The MCP influence on ion selection is of concern for the overall science mission of DANDE since the -2500V potential is a functional response on the gain term for the MCP, lower values will reduce the gain and overall signal, potentially to a threshold where an impact will not be observed by the anodes and digital counting circuitry. However, suppose the MCP voltage was reduced this should

result in a reduced influence of the MCP on the ion selection process and ultimately manifest itself as a change in the energy resolution plot originally seen in Figure 21.

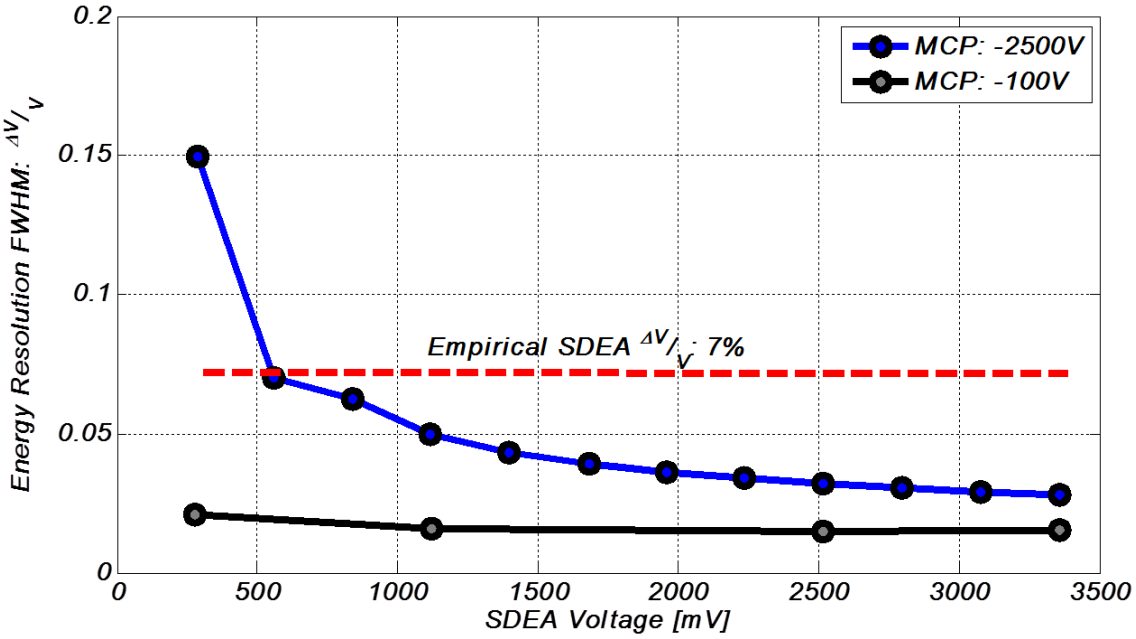

Figure 23 Reduced 2D MCP Voltage

Figure 23 shows how the effect of a reduced MCP voltage, up to -100V bias from the SDEA ground plate versus the original operations scenario of -2500V as an overaly. The system still behaves in a non-linear manner, but the degree at which is does is drastically reduced, in fact is reasonable to suggest that the resolution of the system is roughly 1.5-2% since it is already largely asymptotic. This response to MCP potential calls into question the validity of the 2D simulation, unfortunately the physical system cannot be tested for this sort of response because a gain of 60dB (corresponding to -2500V on the MCP based on manufacturer specs) is necessary for particle detection. With the MCP at a lower voltage now the proportion of passed ions also drops at the peak, though still >95% of ions entering the SDEA are

selected at the peak indicating the high transmission was partly the cause of the MCP potential.

This evidence suggests that a 2D representation of the SDEA is likely not a good candidate the model the physical system. Further review of the process by which the SIMION models a 2D workbench implies it does not consider the system to be truly infinite for the axis into and out of the screen (in DANDE's case the cross-track angular sensing axis). There is reason to believe the software bounds the 3rd dimension as a single unit grid. The impact this has was not directly evident with the parallel plate case study since a secondary perpendicular electric field was not present as is the case with the SDEA and the MCP fields. Since there is already an interplay of the MCP in the SDEA chamber the edge effects which were assumed to be negligible in an ideal case of ions flying down the boresight of the SDEA may have actually had a greater influence due to the lack of shielding provided by the curved enclosure the SDEA. In principle this could explain the divergent energy resolution results in simulation while maintaining a reasonable SDEA factor since the enclosure is largely a field free region (besides the desired SDEA energy selection field) except at the exit aperture.

6.3 SIMION Grid Unit Tolerance Sensitivity

On a side track to the physical system agreement in modeling because the grid sizing is on par with the manufacturing tolerances observing the change in the system due to a forced mis-alignment is warranted to ensure there exist no great sensitivities. Changing the length and height of the SDEA chamber affects the

greatest number of parameters since height deviations would change the gradient at the entrance to the SDEA and length would change the overall integrated force on the ions passing through. These changes should largely be observable through the SDEA plate factor. Table 5 enumerates a range of length variations and the subsequent change in SDEA plate factor.

Table 5 SDEA Length Variation

L [in]	ΔL [in]	D [in]	L/D	SDEA Plate Factor [eV/V]
1.228	-0.057	0.590	2.082	3.41
1.259	-0.026	0.590	2.135	3.51
1.285	--	0.590	2.179	3.58
1.315	+0.030	0.590	2.229	3.64

For this particular dimension the possible mis-alignment is a function of the tolerance stack-up between the ground plate and the deflector plate which can be assumed as a superposition of each of the 0.005" tolerances. This would indicate the max possible deviation in the length of the SDEA chamber of 0.010", the simulated deviation observes situations outside these bounds up to 6X smaller and 3X larger. All of the plate factors described are using the initial assumption of the center SDEA voltage for peak selection at 100% passage. In the original as built run the tolerance on that assumption was 3.1%. Due to intentional deviations the SDEA factor the change is 4.7% lower than the as built spec in the smallest tested dimension of 1.228", a mis-alignment nearly 6X greater than expected by tolerance stack-up alone. On the opposite end of the spectrum when expanding the SDEA to

as large of a length conceived, a 3X greater deviation than expected from tolerancing, changes the SDEA plate factor by 1.7% if the as specified geometry is considered truth.

Consider now a scenario where the tolerance stack up is not a variation in length but height of the SDEA. The normal as built case is with a height of 0.590" is used, but using a figure of merit for the length to height ratio (L/D) from Table 5 a similar set of height deviations can be found and are noted by Table 6.

Table 6 SDEA Height Variation

L [in]	D [in]	ΔD [in]	L/D	SDEA Plate Factor [eV/V]
1.285	0.579	-0.011	2.225	3.81
1.285	0.590	--	2.179	3.58
1.285	0.602	0.012	2.137	3.38
1.285	0.618	0.026	2.083	3.06

Now the relative changes in the dimension are smaller 1X to 3X the expected tolerance stack-up while the compared figure of merit L/D is similar to those tested for length variation. Consider the as built dimensions as truth for a moment and observe the percent deviation in plate factor from this excursion, when the height decreases by the allowable tolerance stack-up of 0.010" a 6% change in plate factor would be expected. The original simulation using uncertainty derived from the voltages with 100% ion passage showed a 3% uncertainty around a 3.58eV/V SDEA plate factor indicating that the unit grid size limitation does not exceed potential change from manufacturing tolerances alone. This quick check indicates that using

a grid size of 0.1mm (~0.004") is an acceptable sizing since there is not a great influence to the system by changes in the internal SDEA chamber geometry. Further the expected deviation when plotted exhibits a linear trend as opposed to a system that would respond non-linearly and be harder to characterize as seen in Figure 24.

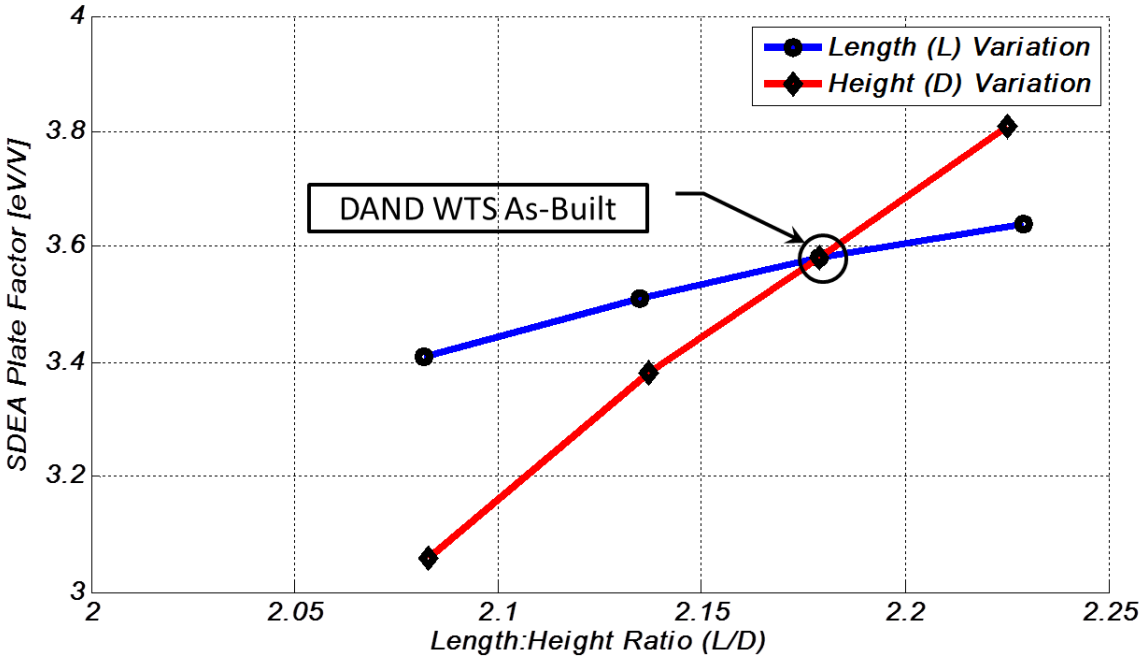

Figure 24 SDEA Chamber Geometry Sensitivity

CHAPTER 7: THREE-DIMENSIONAL SIMULATIONS

Due to the apparent disagreement with the 2D workbench and the data collected during test it was not a stretch to consider importing a 3D CAD model of the WTS SDEA and running the same series of tests on the instrument ion optics to determine the SDEA Plate Factor as well as energy resolution. By using SIMION again a new parameter can be monitored for transmission function or proportion of ions passing through the SDEA at the peak of energy selection.

7.1 Validation of Geometry

Briefly discussed in the 3D workbench build up section was the concept of importing .STL files of parts from an assembly to maintain spatial alignment. The results of this process for the as built SDEA runs are shown in Figure 25 with the SIMION assigned coordinate system in the lower right.

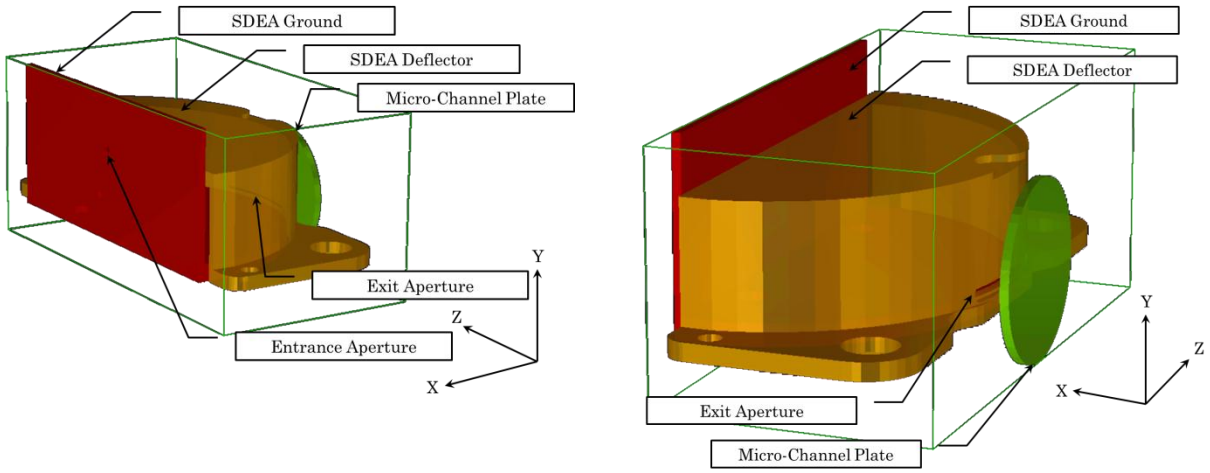

Figure 25 SIMION 3D SDEA Potential Array [8]

During testing runs the impact coordinates were recorded on the X-Z Plane so the ions which passed through the SDEA could first be identified based on the distance

traveled along the X-Axis and then the location on the MCP on the Z-Axis to check for angular distribution.

7.2 Energy Sweep of the As Built System

Performing the same analyses of the 3D system as was conducted for the 2D the first logical point to consider is the proportion of passed ions resulting in counts on the modeled MCP. This is similar to the energy sweep process from Figure 13, however in that case a current was sampled at varying voltages of the SDEA. The current produced is a product of the ion impacts which cannot be reproduced with SIMION. Figure 26 shows the energy sweep of the 3D SDEA model with the individual ion energies called out as the horizontal axis of the SDEA voltage increases.

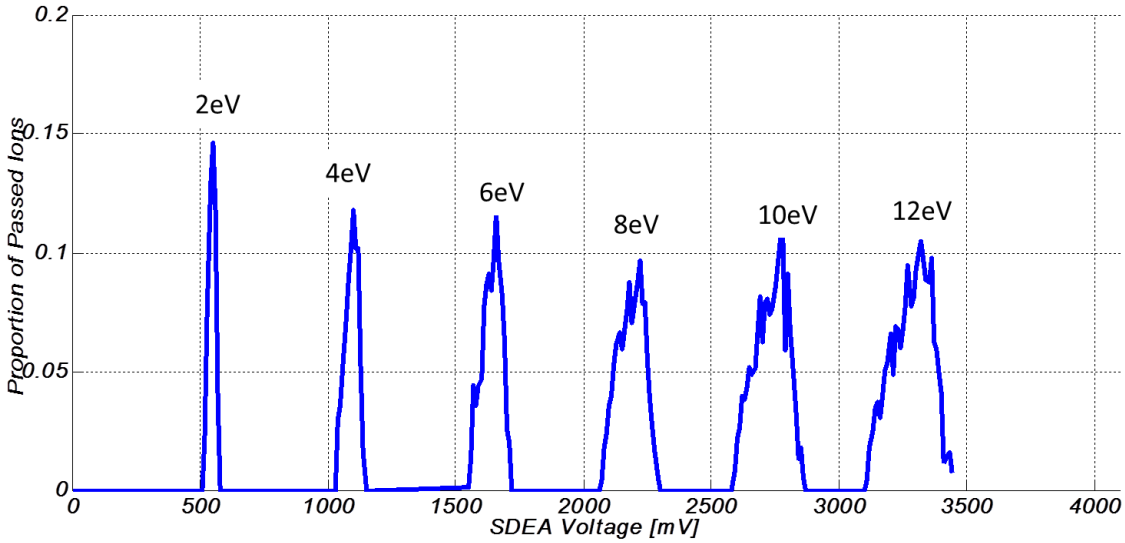

Figure 26 3D Geometry Energy Sweep

There is a dramatic decrease in overall passage of ions through the SDEA in this case compared to the 2D simulations. To that end the overall spread of the ions

despite the uniform energy is visibly smeared across several SDEA voltages at each of the tested energies. This is consistent with the chamber testing as ion energy into the instrument increased.

Further the original simulations and analytic results of the SDEA system suggested that based on the entrance to exit aperture ratio the system could be in a regime of either rectangular or triangular passage of ions. The 2D simulations would appear to indicate that DANDE with the entrance aperture at 0.040" and the exit at 0.013" would be rectangular as assumed by the near 100% passage and steep attenuation on either side of the selected region. However, due to the inconsistencies in energy resolution this assumption is called into question. With the 3D case a triangular region of passage is observed, albeit at a low proportion of overall selected ions, but none the less consistent with the design rules of thumb from GSFC.

7.3 SDEA Plate Factor

Moving to the first performance metric of choice the SDEA Plate Factor for the peak energy at the passage, this is described by Figure 27.

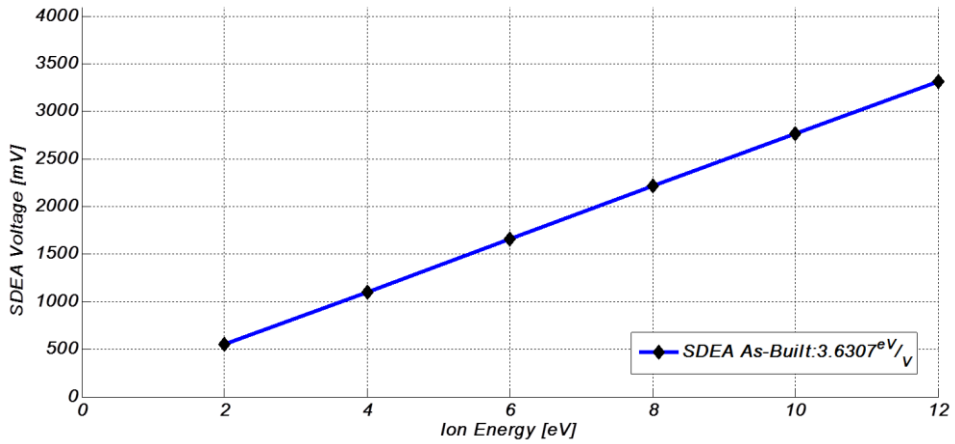

Figure 27 3D Geometry SDEA Plate Factor

An observed plate factor of 3.6eV/V is right on in comparison to the empirical test campaigns at Goddard. What is more interesting about this and its agreement with the empirical testing is when considering that while the 2D test results did fall in this range that was without a discernible peak. The 2D cases observed 100% passage across a range of SDEA voltages and it was assumed that the peak was in the center. Visual inspection of the 3D case energy sweep in Figure 26 would indicate that often the peak is not in the direct center of the energy pass band, but rather shifted off-center towards the latter half of the pass band.

7.4 SDEA Energy Resolution

The final observable figure of merit for comparison to prior testing is the overall resolution in the energy spectrum. Recall that with chamber testing of the proto-flight unit using the same ion optics the resolution was ~7%. That is to say variations in temperature have to exceed 7% of the overall energy of the species under observation to be detected. With the as built system imported to SIMION the observed energy resolution is shown in Figure 28. While there is observable

spreading of the selected energy region it is consistently proportional to the input energy under examination at the time.

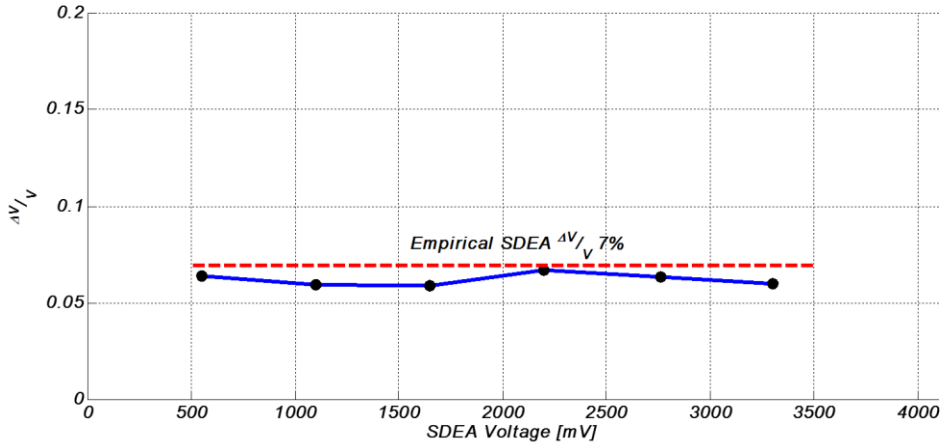

Figure 28 3D SDEA Geometry Energy Resolution

There is some variability in the data sets since the ion trajectories from one test to the next energy are not identical and there is some observable fluctuation. Interestingly the as build system has very near identical performance of the model to the truth data at just about 6.5%. Recall this metric is derived from the full width at half max, so the peak detected for the SDEA plate factor is halved and the intersection of that value on the upward and downward swings of the energy spectrum are recorded.

7.5 Model Predictions Validation

After considering the outputs of the 2D profile workbench model and then moving into a 3D workspace capturing the curvature of the SDEA there is a large disparity in agreement between the two with the physical system. Both map to a SDEA Plate Factor that is reasonable, but then completely different energy resolutions. Suppose then the 3D workbench more accurately predicts the truth

measurements of the flight instrument due in large part to the way in which the 2D workbench approximates the infinite axis as not truly infinite but a finite set of grid points in the potential array as discussed. The 3D workbench then could be modified to more accurately represent the "far field" effects of the 2D SDEA profile of a CAD model were created that eliminated the curved geometry and solid walls on the side of the SDEA. This sort of finite SDEA profile in the 3D workspace is depicted in Figure 29. The same series of tests can be run on the SDEA in this configuration, should it match up to the original 2D workspace results this would suggest there is a geometry mismatch in the SDEA where the electric field in the SDEA chamber is influenced by the geometry of the SDEA as opposed to the flight path of the ions being largely unaffected as would be the case for a simplified parallel plate capacitor. Alternatively the SDEA profile could align more to the 3D workspace results above in which case there is an inconsistency in SIMIONs analysis of the 2D workspace.

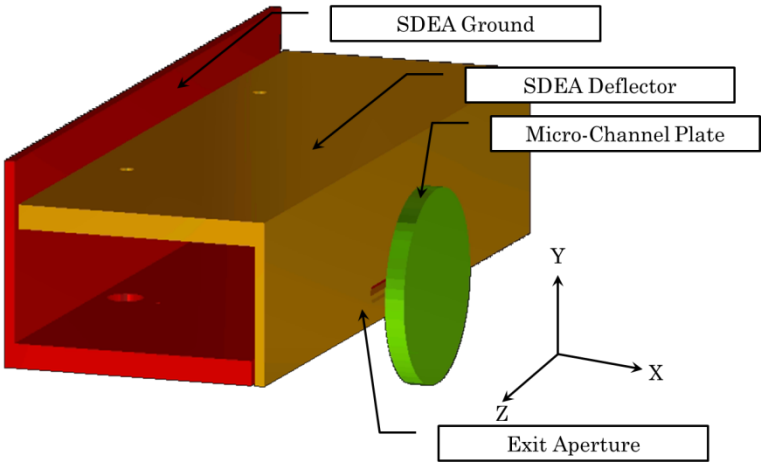

Figure 29 SDEA Profile Geometry

Figure 29 shows a representative geometry sample where the entire length of the SDEA along the assigned Z-axis from SIMION is 4", additional scenarios were considered where the total length was up to 6" and as small as 1". The 4" profile case acts as a means to test the effect of moving from a curved SDEA that has a constant distance of travel across the SDEA to a design that maintains the same major dimensions, but removes curvature from the equation. The 1" case considers a scenario where the electric field from the MCP is not entirely shielded from the SDEA chamber since the walls of the SDEA do not extend beyond the major dimension of the MCP.

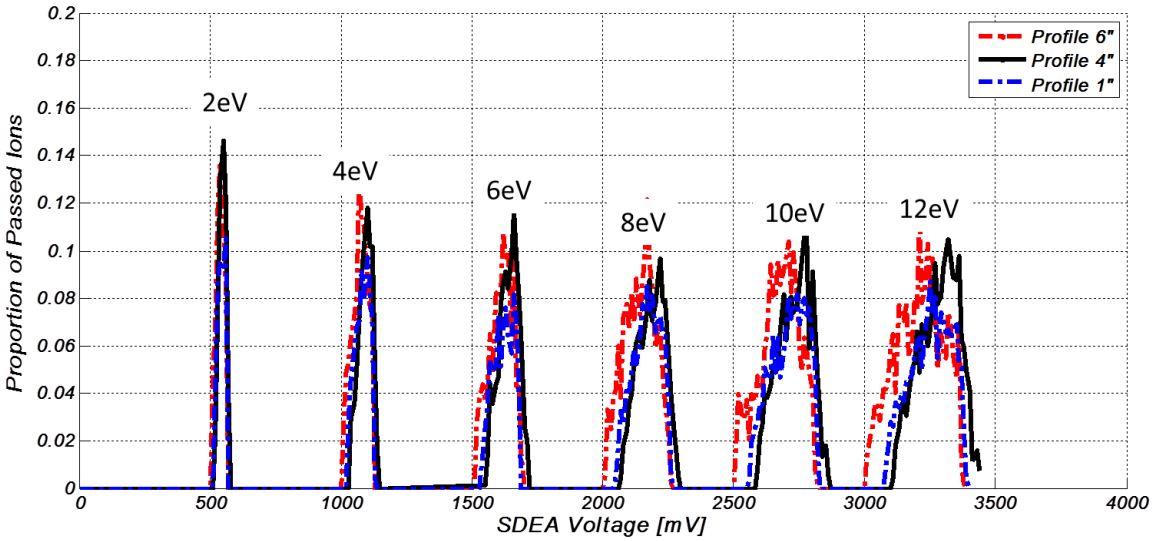

Figure 30 SDEA Profile Ion Passage

Figure 30 shows the transmission of ions at different test energy cases for the 3 profile cases considered. Upon visual inspection all three cases are self-consistent with the total ion passage proportion as well as the location of the peaks indicating that the SDEA Plate Factors will be largely the same, and they are at ~3.6eV/V.

Further the total passage of ions is in line with Figure 26 for the as built geometry in the 3D workspace. Since there is no observed 100% passage this calls into question further the validity of the 2D results. To that end an interesting question is raised as to what is the physical mechanism to achieve 100% passage of ions. The entering beam will have the same diameter as the SDEA entrance aperture and to have 100% ion passage the beam would have to be focused to at the very least less than or equal to the dimension of the exit aperture. In the 3D case where there is an average of 10% passage at any given time then it would indicate there is not optimal focusing of the ion beam in the SDEA, either the focus has not yet occurred, or the focus is inside the void of the SDEA chamber away from the exit aperture.

Since the proportion of passed ions indicates the profile approximation in 3D matches the as built system the sensitive parameter that originally stood at odds in the 2D workspace was the energy resolution, Figure 31 shows the energy spectrum response for the profile cases considered.

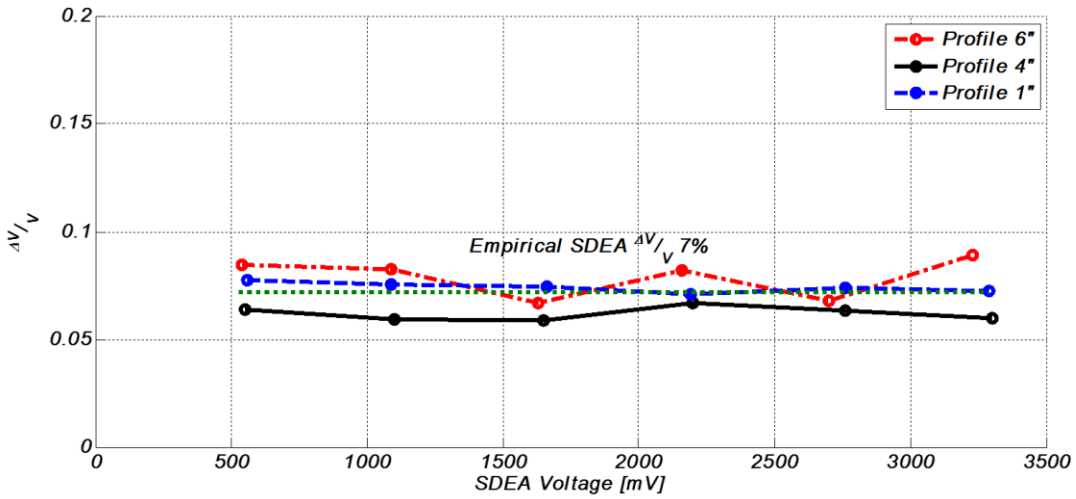

Figure 31 SDEA Profile Energy Resolution

By and large the resolution of the 3 profiles depicted fall in line with the empirical testing results with some excursions higher and lower, but not as dramatic as was the case with the 2D workspace. At present then the results of modifying the geometry of the 3D SDEA system to mimic the profile testing of the 2D workspace shows the second hypothesis of the 2D standing at odds with the flight instrument to be the most likely conclusion to draw. With that being the case there is the troubling implication that total ion passage is less than optimal where at the peak only 10% of the ions on average can be selected.

Identifying a key contributing factor to the passage of ions should be addressed since it has operational impacts to the flight system in terms of integration time to achieve a reasonable number of counts which drive error terms down as discussed in Table 2. Figure 32 shows a cross section of a general population ion flight through the 3D SDEA with an overlay of the quadrants of the chamber. The ion beam focal point appears to be in the upper left-hand quadrant of the SDEA. This premature focus results in the beam diverging as it approaches the SDEA exit and noted in the graphic in red are the ion impact points. The beam has become so wide that most of the ions impact the back wall of the SDEA. As mentioned earlier the distance along the back wall of the SDEA maps to the energy spectrum since as the potential is increased with the SDEA scan ions impacting the back are eventually shifted down vertically ultimately to a point where they are able to exit and impact the SDEA. This beam spreading though gives rise to the energy resolution limitations discussed in each test scenario.

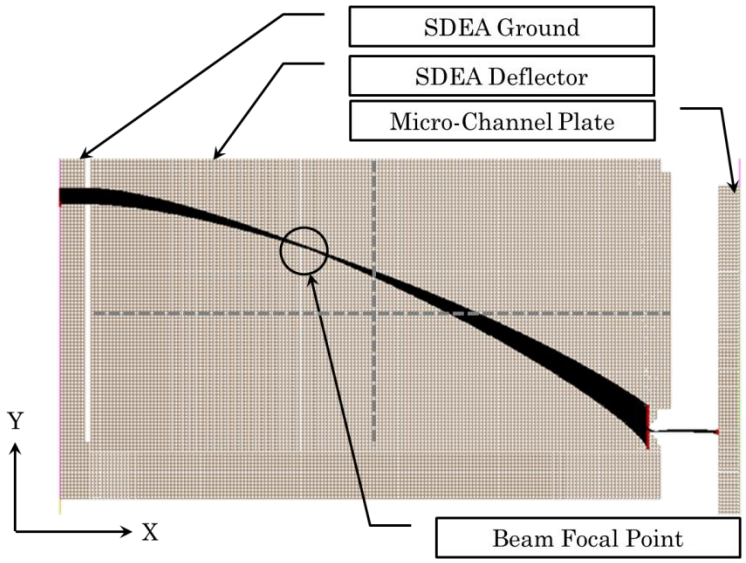

Figure 32 3D Cross-Section of Ion Flight Paths

The nature of the SDEA having the two opposing potentials right next to each other at the entrance and exit of the chamber presents on possible avenue to consider. At the entrance aperture the gradient of the potential is much stronger at the top of the entrance than at the bottom despite the aperture only being 0.040" in diameter. As articulated in Equation 3 the forcing of the ions is directly affected by the gradient of the potential field. This would mean that the ions at the top of the beam would experience a greater force than those at the bottom which in of itself gives rise to the focusing. It would stand to reason then if the entrance aperture and subsequently the boresight of the instrument where lowered away from the chamber ceiling constrained by the SDEA deflector that the premature focusing could be moved to the exit aperture. This is the case presented in Figure 33 where the distance from the floor of the SDEA to the entrance is shifted first 0.050" and then 0.150" from the original 0.685" as built specification.

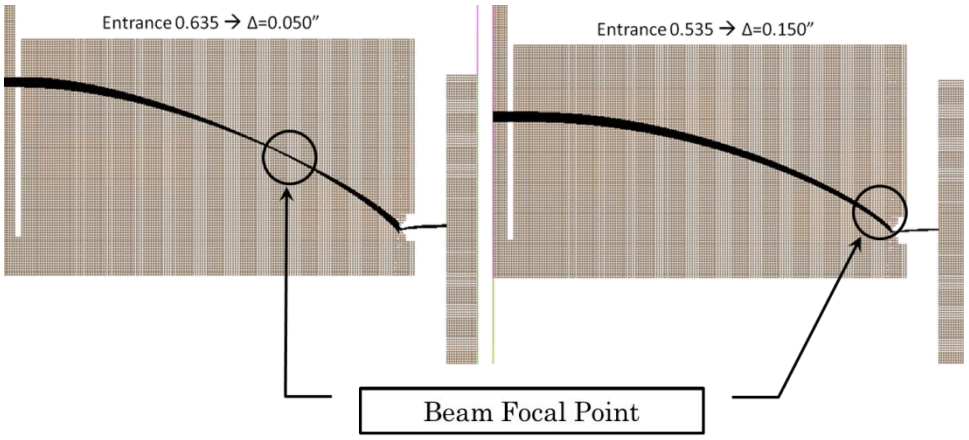

Figure 33 SDEA Cross-Section with Entrance Aperture Shift

Now the divergent beam on the back wall of the SDEA is greatly reduced just by visual inspection alone, but the change is even more dramatic looking with the energy resolution graph in Figure 34. The largest shift of 0.150" shows the focal point very near the exit aperture, and in the test of the energy resolution exhibits the consistently lowest energy resolution at approximately 1.5%.

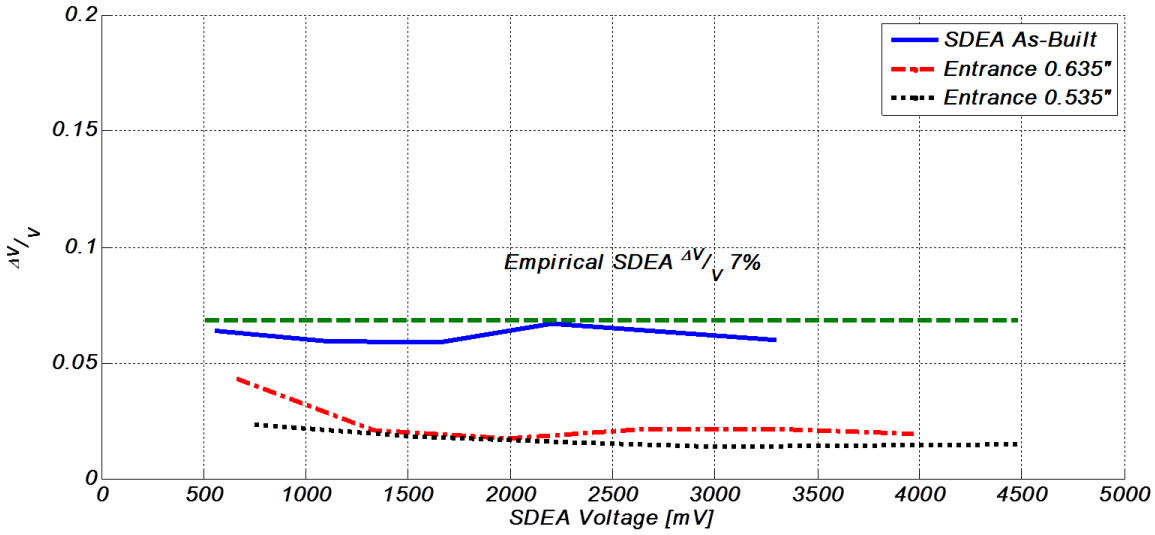

Figure 34 Energy Resolution with Lowered SDEA Entrance Aperture

Recall that the observed output of the 2D workspace runs was at or around the same performance metric, and it observed 100% passage. Consider then the SDEA geometry tested here where the lowest resolution has been reduced there should be a subsequent change in overall passage of ions.

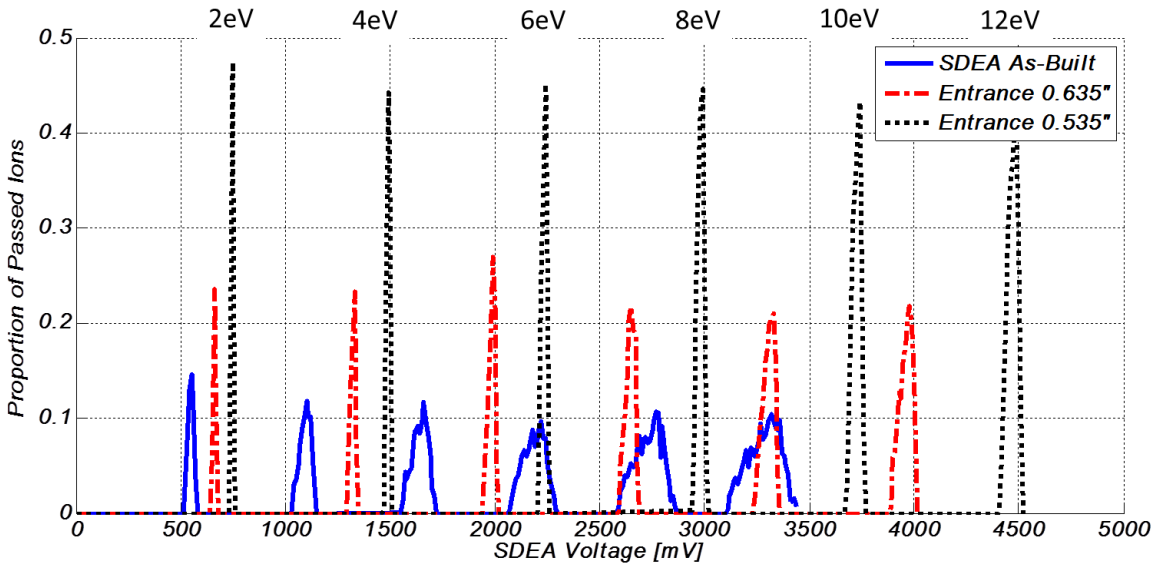

Figure 35 SDEA Entrance Aperture Shift on Ion Passage

Figure 35 shows that as the energy resolution decreases the overall proportion of ions increases. At the lowest point for the entrance aperture there is on average 45% of the total available ions at the peak selected by impacting the MCP. There is also a dramatic effect on the energy selection. Now that the gradient has been reduced the energy spectrum has been spread out along the range of voltages the SDEA would need to scan directly impacting the SDEA Plate Factor. Recall that the as built system was tested and simulated to have a plate factor between 3.6-3.7eV/V, at a shift of 0.050" downward from the as built system the plate factor drops to 3.0eV/V and then one step further at 0.150" the plate factor is 2.7eV/V.

This would mean any alterations to future instruments in this regard would need to account for SDEA voltage range changes, but they are manageable since to still observe the 1-12eV energy spectrum a max voltage of 5V would be required.

It appears there is a logical explanation of the low transmission for the as built system due to the gradient of the SDEA potential at the entrance. And further the performance that was observable in chamber testing matches with the SIMION modeling outputs. Overall then the modeling SIMION is capable for more complex systems like the DANDE WTS and specifically the SDEA is rooted in reality. This can have far reaching benefits to the operations concept for DANDE and the WTS once it is on orbit as well as future iterations of the instrument being tested in SIMION prior to cutting metal and having a baseline expectation of how such ion optics should behave once ready for testing.

CHAPTER 8: WTS INSTRUMENT RESPONSE

Under the operating assumption that the pass-band features of the 3D SIMION simulations are real there is a desire to understand the overall impact to sensing the environment for DANDE operations. Recall from Table 2 that total observed counts maps to the ability to fit a Maxwellian distribution and invert the data to determine the wind vector, temperature, and relative number densities of the atmosphere. With the reduced efficiency to pass ionized-neutrals there is cause for concern as to the operability of the instrument on orbit. A semi-empirical model for the flux of particles into the instrument can be created and observed efficiencies can be created for the ionizer, SDEA pass-band, and view factor of the peak anode.

The method by which a semi-empirical model can be created for this procedure would be to consider a no wind scenario and all species are "energized" by the velocity difference of the spacecraft and static atmosphere at some temperature. This will ultimately create a distribution of particles that is Maxwellian in nature [2]. That distribution is ultimately subtended by the solid angle of the instrument aperture defined by the collimator as Equation 8 [4]. Where α and ß are the vertical and horizontal fields of view respectively.

$$\Omega_c = 4\, asin\left(\sin\frac{\alpha}{2}\sin\frac{\beta}{2}\right) \qquad \text{Equation 8}$$

This will oppose the free-stream solid angle described in Equation 9. Where the term γ represents the field of view for the flow.

$$\Omega_f = 4\pi \sin\frac{\gamma_f}{2} \qquad \text{Equation 9}$$

The flow field angle can be described by the magnitude of the bulk velocity due to the spacecraft movement through the atmosphere and the perpendicular components of velocity rising from thermal energy then the maximum angle this creates between the two.

$$\gamma_f = \operatorname{atan}\frac{V_{thm}}{V_{mag}} \qquad \text{Equation 10}$$

The relation of thermal energy and velocity described earlier can be found given the Boltzman Constant and atmospheric neutral temperature. The ratio of the two solid angles, collimator and free-stream flow, give rise to the steric factor which relates the flux of the atmosphere to the view angles of the instrument shown in Equation 11 providing a flux into the WTS instrument [7].

$$\Phi_{WTS} = \Phi\left(\frac{\Omega_c}{\Omega_f}\right) \qquad \text{Equation 11}$$

The flux outside the instrument can be described by [4].

$$\Phi = nAV_{thm}\frac{e^{-s^2f^2} + sf\sqrt{\pi}(1 + \operatorname{erf} sf)}{2\sqrt{\pi}} \qquad \text{Equation 12}$$

The scalar coefficients s and f which are the ratio of bulk to thermal speeds and the unit vector of free-stream with respect to the aperture plane respectively. Since the case being considered here is a static atmosphere with the satellite moving through it f will become 1 in line with the boresight of the spacecraft instrument. The equation is led by terms for the number density of the constituents under measurement and the area of the limiting aperture of the instrument, in this case the SDEA entrance.

Now with a way to formulate the flux of particles into the entrance aperture to the instrument as a whole an understanding can be developed of the overall attenuation to the flux from the ionizer, SDEA, and view factor of the anodes. Each of these contributing factors can be assessed as an efficiency of the flux, so the total flux onto the anodes would be described by Equation 13.

$$\Phi_{\text{Anodes}} = \Phi_{WTS}\epsilon_{ionizer}\epsilon_{SDEA}\epsilon_{Anode} \qquad \text{Equation 13}$$

Each of the scalar efficiencies can be deposed based on the effective chamber from Figure 6 and knowledge of the WTS system. $\varepsilon_{\text{ionizer}}$ stems from the efficiency at which the WTS instrument ionizes the neutral particle flux. The development of this efficiency is beyond the scope of this work, but is suggested to be 0.1-0.01% of the particles passing through the electron beam.

The $\varepsilon_{\text{SDEA}}$ term represents the pass-band selection efficiency determined through 3D SIMION testing, and the fraction of which the Maxwellian Energy distribution is selecting the ionized-neutrals. What first must be considered to produce this result is a numerical way to represent the pass-band. Figure 36 shows the pass-band regions as a function of energy represented as triangles. Now the peak passage proportion can be assessed along with the width of the pass-band along the ascending or descending edges.

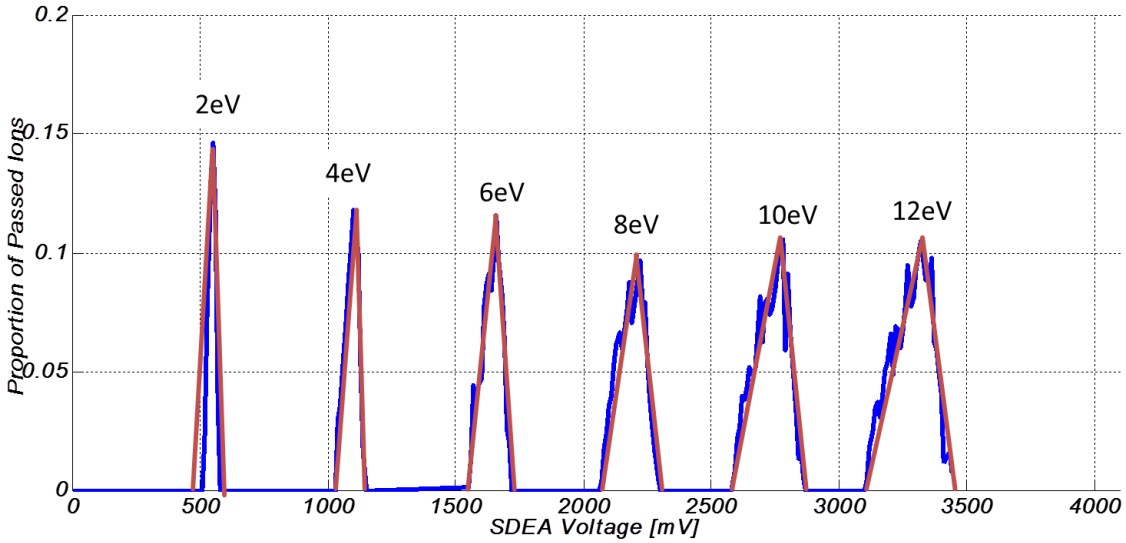

Figure 36 SDEA Pass-Band Approximation

Figure 36 in of itself does not fully describe the passage through the SDEA and the probability of selection. Instead this must be effectively super imposed on the Maxwellian energy distribution which is described by Equation 14 [4]

$$\Pi_{\mathrm{m}}(\mathrm{E}) = \frac{nE}{\sqrt[3]{2\pi k_b T}\sqrt{m}} e^{\left(\frac{-\left[E-2\sqrt{E\bar{E}}+\bar{E}\right]}{k_b T}\right)} \qquad \text{Equation 14}$$

The true efficiency for the fraction of particles sampled at any given SDEA potential, or selected energy, would then be described by Equation 15.

$$\epsilon_{\mathrm{SDEA}}(E,V) = \int_{E_{Low}}^{E_{High}} \Pi_{\mathrm{m}}(E) S(E) dE \qquad \text{Equation 15}$$

Integrating across the entire energy spectrum captures the continuum distribution of the Maxwellian (Π_{m}) and the pass-band efficiency of the SDEA (S). The efficiency of the pass-band can be described as a piece-wise function for the ascending, descending, or off peak energies shown in Equation 16.

$$S(E) = \begin{cases} \frac{2}{d \cdot E_C}(E - E_L) & if\ E_L < E < E_C \\ 1 - \frac{2}{d \cdot E_C}(E - E_C) & if\ E_C < E < E_H \\ 0 & if\ E_L > E > E_H \end{cases}$$

Equation 16

The center energy is represented as E_C, the low and high side of the pass-band is shown as E_L and E_H respectively, finally d represents the full pass-band width. For the purposes of the integration process E_C would be selected based on the energy of the species under test at the moment and the properties of d, E_L and E_H would be functions of E_C which can be characterized across the energy spectrum from Figure 36.

For these purposes to characterize the magnitude of the ε_{SDEA} atomic oxygen and molecular nitrogen are the primary constituents of the atmosphere studied, from Figure 8 a small cross-section of the atmosphere from 250-500km is analyzed for the primary constituents showing O and N_2 are dominant. Consider Equation 14 again and notice that it is a strong function of the particle properties, specifically number density (n), mass (m), and atmospheric temperature (T). The NRLMSISE-00 atmospheric model allows for number density and temperature to be computed as a function of altitude, so a flux value that is already altitude dependent become compounded again by these factors. Figure 37 shows the atmospheric neutral temperature profile as a function of altitude and provides bounds for analyzing the ε_{SDEA} function.

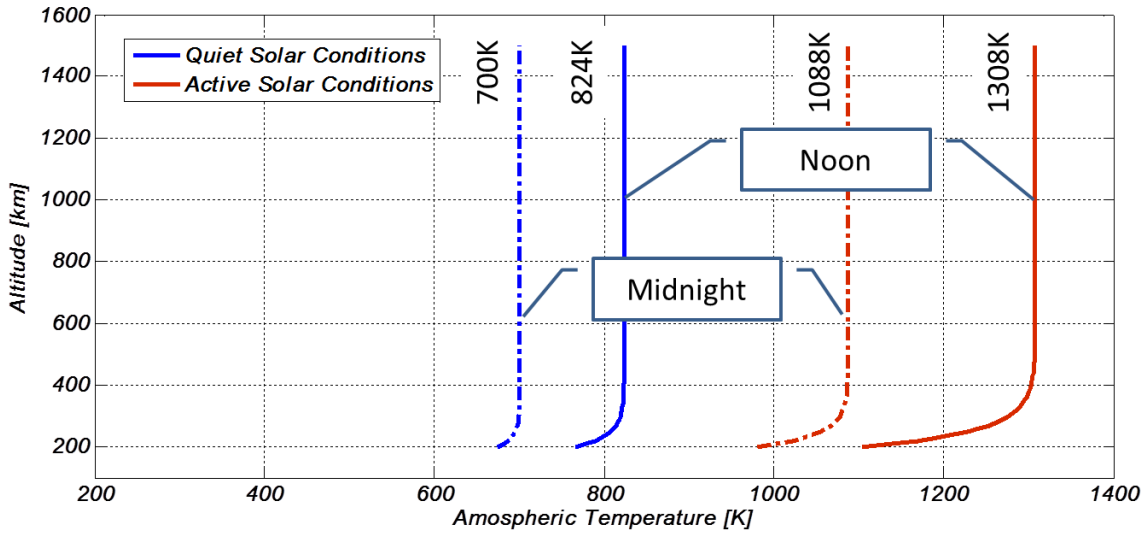

Active:	Quiet:	Location:	Time:
F10.7 = 200sfu	F10.7 = 75sfu	Lat: 0	Date: 2012 Day: 150
Ap = 20	Ap = 5	Long: 0	Midnight & Noon

Figure 37 Atmospheric Neutral Temperature Profile

Using a range of 500-1400K temperatures going from the coolest midnight during solar minimum conditions up to the hottest noon during solar maximum conditions provides a good bound for the potential scenarios DANDE may see during its orbit lifetime. The behavior of ε_{SDEA} is summarized in Figure 38 where from the coolest conditions considered at 500K up to the hottest conditions of 1400K the difference is 0.8% with an average for O of 1.61% and N_2 of 2.07%. Molecular nitrogen exhibits a consistently higher fraction of passage since another parameter to the input of the Maxwellian is mass, but recall over the column of the atmosphere under consideration there is significantly less molecular nitrogen compared to atomic oxygen due to the differing scale heights.

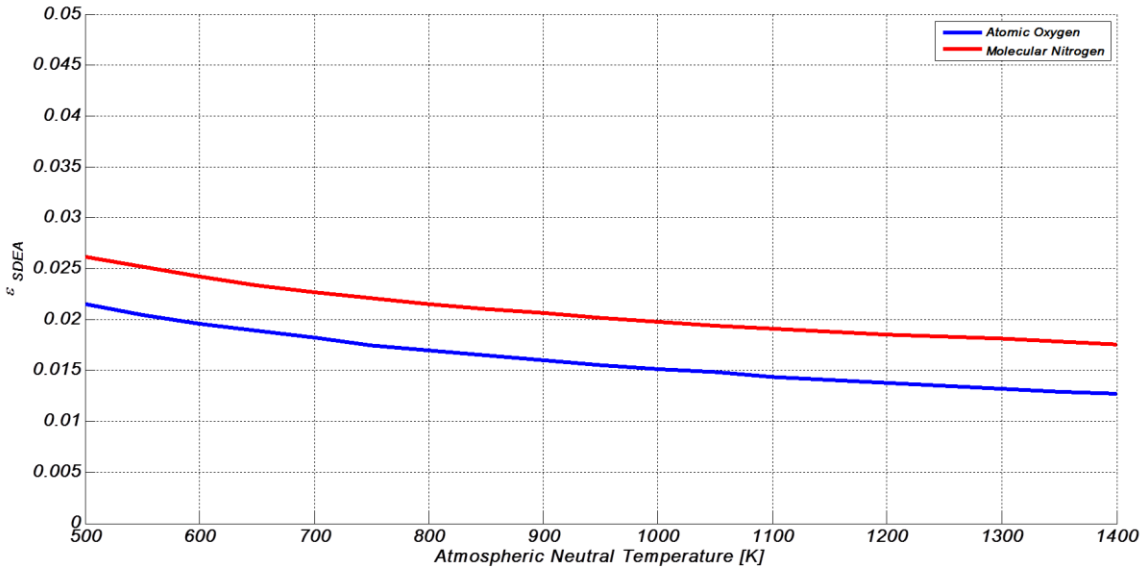

Figure 38 SDEA Selection Fraction Temperature Profile

This effectively bounds the term for ε_{SDEA} and for the purposes the average condition will be used to estimate the flux onto the anodes and the estimated counts at the peak.

The final item to consider is similar to the subtended entrance aperture, but exists at the anode. The Maxwellian distribution describes the spread in energy space, but that does not capture the spread of particles over the spatial dimension of the anodes. For this estimate a flux on the anodes will be considered only at the location of the peak, since there is no wind this peak will occur at the boresight of the instrument. The anodes and their respective fields of view are illustrated by Figure 39. Notice down the boresight there is not one anode in the center, but one on either side of boresight.

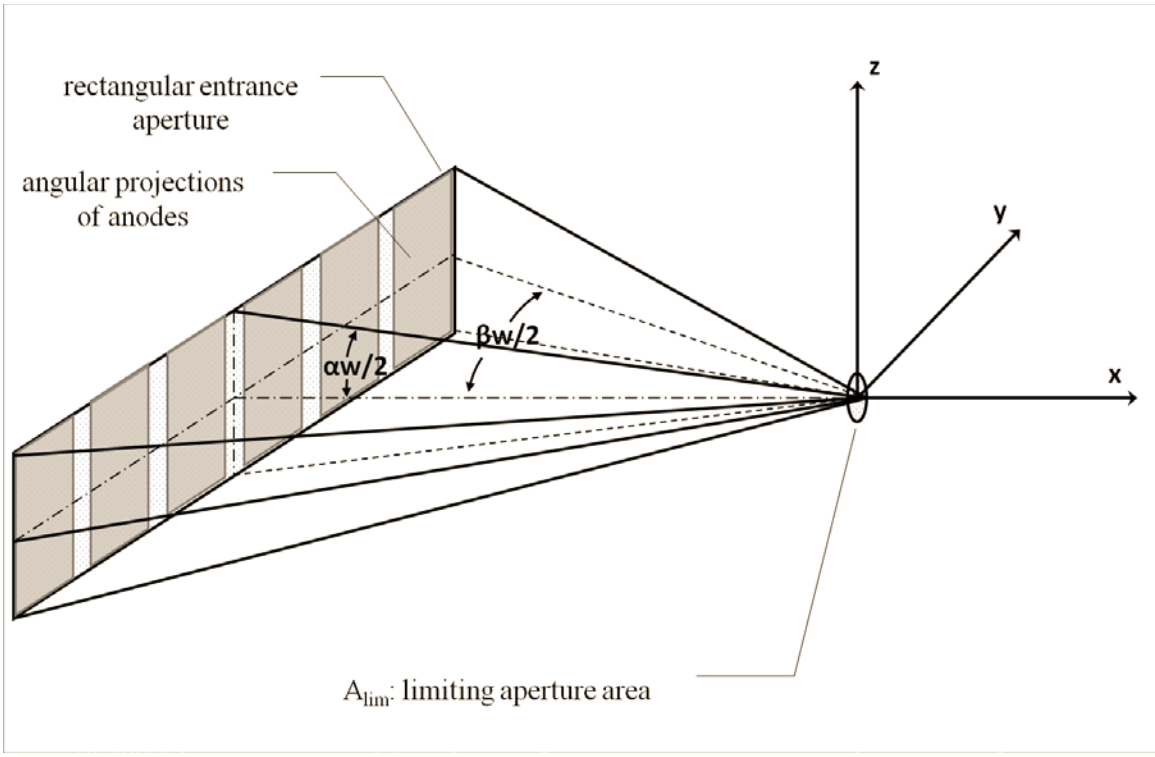

Figure 39 Anode Field of View Projections on Particle Flow [4]

There are 12 anodes in the DANDE WTS instrument so each represent ~2.5° of the field, neglecting empty spaces between anodes. Instead of just integrating for a set period of time to determine the total counts at the anode plane it is important to consider the counts at the peak and subsequently only consider the counts on the anode corresponding to the peak. Since the anode plane with respect to the boresight is symmetric the distribution of particles given by Figure 40. To estimate the flux of particles onto an anode in the center of the distribution the ratio of the area under the field of one anode compared to the full spatial distribution must be consider. The full spatial distribution though is dictated by γ_f which is a function of temperature since it is the angle between spacecraft velocity and thermal velocity.

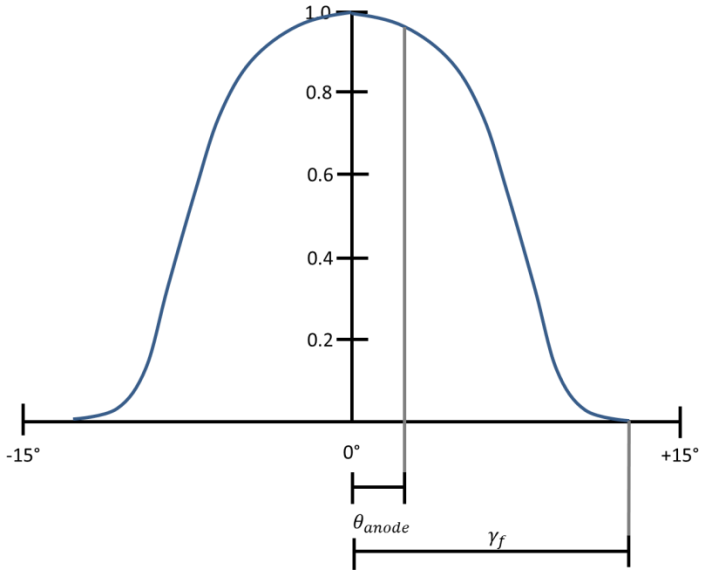

Figure 40 Particle Distribution on the Anode Plane of WTS

This distribution can be approximated by a cosine function of the form seen in Equation 17.

$$\epsilon_{\text{anode}} = \frac{\int_0^{\theta_{anode}} \cos\frac{180\theta}{2\gamma_f}\, d\theta}{2\int_0^{\gamma_f} \cos\frac{180\theta}{2\gamma_f}\, d\theta} \qquad \text{Equation 17}$$

What will end up happening is as mass increases and/or temperature decreases the distribution of particles spatially will decrease causing an increased proportion of particles to impact the anode plane near the center anodes. The decreasing temperature resulting in an increasing proportion is the opposite response of overall flux into the instrument in cooler conditions since the overall number density will have decreased disproportionately. Since the free-stream flow angle varies as temperature it will be examined on a case by case basis following the temperature profiles of Figure 37.

Now all the pieces are in place to estimate the flux of particles onto the anode plane, and more specifically onto the central anode itself. The flux of particles is examined at each stage of the instrument in Figure 41. Here the behavior of O is examined. The black line represents the flux into the instrument aperture when the flow solid angle is subtended by the instrument aperture. Then in red the flux is reduced by the ionization efficiency. Blue represents the flux after the particle selection process in the SDEA when the pass-band subsamples the Maxwellian Distribution. Finally the green on the far left represents the spatial distribution integrated over just the view factor of the center anode which will line up with the peak counts.

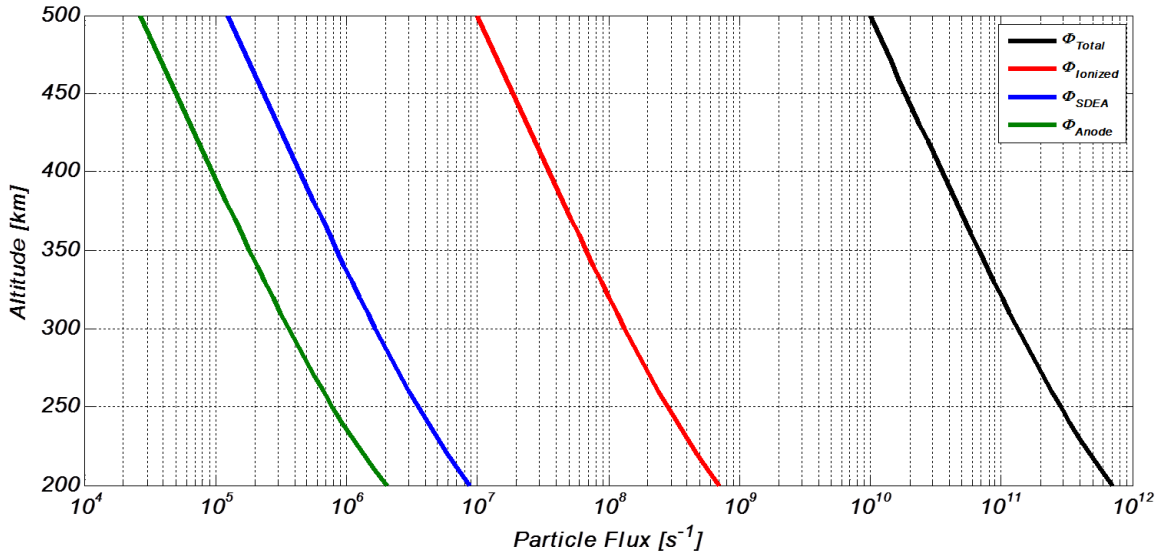

Figure 41 Atomic Oxygen Flux Through WTS

Molecular nitrogen exhibits the same behavior of decaying particle flux through the instrument, but due to its original number density being less than that of atomic oxygen in the atmosphere the overall flux is decreased.

Consider now the operations aspect of this instrument. At each energy step in the 20 step scan the system will integrate collecting counts for 1ms, now knowing the flux on the peak count anode will allow for an estimate of the total peak counts in different atmospheric conditions. Suppose the same atmospheric conditions are examined for the atmosphere as was simulated for the neutral temperature profiles above. Active conditions would simulate geomagnetic activity during solar maximum (F10.7 = 200 sfu, Ap = 20), and quiet conditions represent solar minimum (F10.7 = 75sfu, Ap = 5). The overall particle count would result in Figure 42 when considering solar max and min conditions.

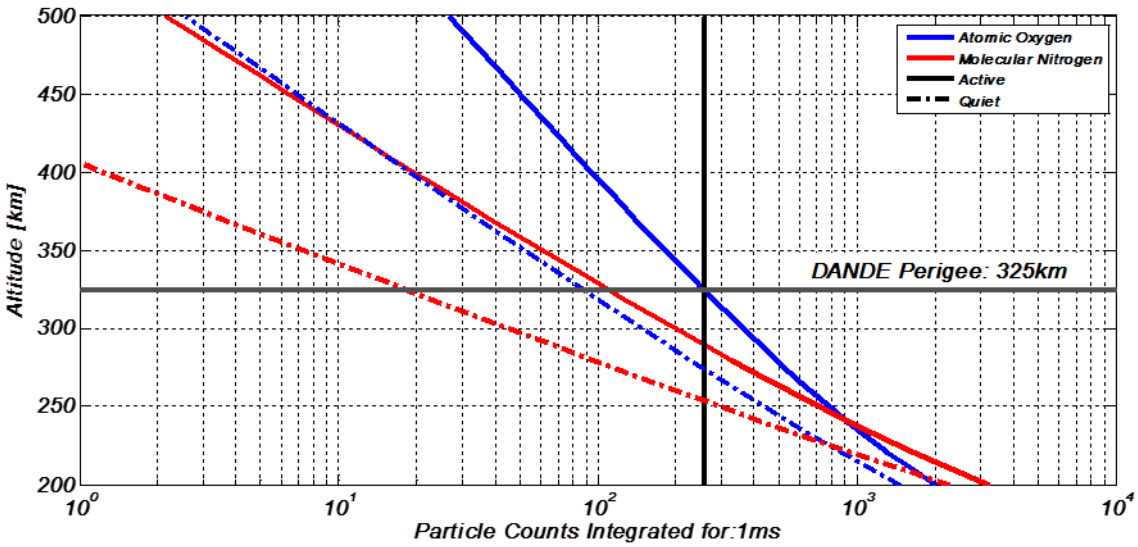

Figure 42 Estimate Particle Counts at Peak for DANDE WTS

Also show on the horizontal is the DANDE initial orbit perigee, which will decay over the period of the orbit, but suggests the floor for atmospheric density at the initial orbit insertion point. Also vertically is the black bar at 256 counts, this is the point at which the counter circuitry of the WTS instrument will roll over

causing an ambiguity. Solid red/blue lines represent the overall particle counts for 1ms of integration for molecular nitrogen and atomic oxygen during active geomagnetic conditions. Dashed red/blue lines represent the particle counts during quiet geomagnetic conditions. By visual inspection for the orbit that DANDE will be inserted to under active conditions oxygen will approach the counter limit for a single integration at perigee, but at every altitude greater than perigee DANDE will struggle to achieve a reasonable number of counts. The instrument noise floor is not known at this time, and a likely flight experiment will be to run the instrument during a climb from perigee to apogee and determine when it is no longer possible to observe counts under this flight condition. This analysis can be consider with Table 2 WTS Peak Counts Error Break Down for 10m/s wind magnitudeTable 2 to provide an overall error estimate when discerning the validity of the on orbit datasets returned form the spacecraft.

CHAPTER 9: CONCLUSIONS

The overarching purpose of this work is to take a second look through the DANDE WTS instrument ion optics and provide evidence that SIMION can properly model the complex geometry. Thus far two and three dimensional boresight simulations have been conducted mimicking the testing and data products of the flight instrument prior to spacecraft delivery. Proving SIMION acts as an acceptable proxy to vacuum chamber testing allows for intangible data products to be observed as well as constraining the input signal to uniform distributions in energy and velocity which are not possible through chamber tests. This allows for SIMION scenarios to bolster the observed data products from testing since ion injection cannot be as tightly controlled.

9.1 Ion Optics Simulation Validation

Based on the performance metrics that were observable during testing in vacuum with proto-flight and flight instrument optics as well as electronics a energy transfer function and ultimate resolution in the energy space could be developed. Resolution to individual count threshold is more a function of the supporting electronics which is beyond the scope of the optics influence for this work. Several sets of chamber tests were run under different electronics configurations, but all yielded the same overall optics performance.

The first attempt at modeling the SDEA takes the concept that the radial component of particle flow through the instrument is nearly constant and assumes that the profile of the SDEA as the simplest geometry, Figure 18. This shows

agreement to energy selection, but not to energy resolution of the truth measurements from the flight instrument. Upon further review what appears to be in play is the method by which SIMION assumed the infinite axis in the 2D workbench. Unit grid points are used on the assumed infinite axis when calculating the electric field and subsequent forcing on a charged particle. The implication is that while in the flight instrument the SDEA is an external field free region effectively shielding the effects of the MCP potential from the energy selection process. This 2D workbench does not properly capture this since the edge of the MCP is not shielded by the structure of the SDEA deflector. It appears that this manifests as a influence of the MCP in the SDEA chamber by having the 0V equipotential observed near the exit aperture causing the greatest forcing on charged particles to be the potential from the -2.5kV SDEA. One method to mitigate this result is to reduce the MCP voltage, however operationally the MCP voltage is correlated to the gain observed on the data collection anodes. The only course of action to combat this in simulation would be to move into a 3D workbench environment that can emulate the shielding the SDEA deflector provides to the MCP since adjusting the MCP voltage is undesirable from a configuration management standpoint.

Moving into a 3D workspace because of the implications of the improper simulation in 2D actually had an added side benefit of using the spatial referencing of a CAD tool as opposed to by hand ensuring correct geometries. As built models could be imported to SIMION directly and run through the same boresight particle

flow scenarios as the 2D and the vacuum chamber testing of the physical system. In these cases the overall performance that could be measured matches for both the energy conversion and resolution. A startling fact was then uncovered where the total number of observed particles at the peak transmission is extremely low (~10-15%) compared to the total number of particles entering the chamber. This low transmission function aligns well with observed response of the system when performing end to end tests where integration times orders of magnitude longer than the flight 20ms scans were required to have any observable counts.

A major factor in play was hypothesized to be the proximity of the entrance aperture to the roof of the SDEA chamber bounded by the deflector. The thought process followed that particles near the top of the entrance aperture and subsequently closer to the deflector upon entering the SDEA would have larger forcing due to the stronger potential than those at the lower portion of the entrance aperture, this results in premature focusing in the chamber and a divergent beam impacting the back wall of the SDEA. SIMION acted as a beneficial tool for this since quick changes in CAD could be quickly imported and run at varying entrance aperture locations, something that is not possible with a vacuum test with physical hardware. Ultimately the logic flow identified matches the resulting SIMION scenario and ideal focusing could be achieved by dropping the SDEA entrance aperture resulting in approximately 45-50% particle passage at peak selection.

There is substantial evidence to suggest that a three-dimensional workbench in SIMION properly models the dynamics of the DANDE WTS instrument and can

be used in the future to drive operations concepts for the instrument as well as the considerations that go into the data inversion process itself. Even more forward looking there is the potential to use these types of simulations to direct development efforts of instrument optics designs prior to cutting metal and potentially reducing the testing costs since a baseline understanding of the measured results should be feasible to generate with this tool.

9.2 Current Instrument Operational Considerations

At the highest level accepting that the three-dimensional simulation does illustrate the dynamics of the physical SDEA in the DANDE WTS then the two major performance metrics that can be observed are an energy conversion factor of 3.6eV/V and an energy resolution of very nearly 7%. Recall that the operational instrument scans the energy spectrum in 20 discrete steps and that the primary constituents in the atmosphere are O and N_2. It would be most desirable to have the SDEA scan and hit these two peaks in energy since they will result in the strongest signals, as was described in Table 2 total observable peaks is the key driver to the error associated with all WTS style instrument measurements. SIMION models of this instrument setup could in principle be used with atmospheric simulations to test conditions and use cases for data inversion tools by which data off of the spacecraft will be measured after launch. The benefit of SIMION constraining the test environment to user defined inputs can help to direct development efforts in ground processing software.

Interestingly the optics limit the energy resolution and ultimately the discernible temperature accuracy seems to be limiting as opposed to the required number of counts to observe the temperature from an ideal continuum again derived from the error associated with a measurement based on the total number of counts achieved at the peak. This does not take into account one of the key derived performance metrics from SIMION though of how well the SDEA transmits the signal. Since the as built unit has a transmission function of 10-15% at the peak and a scan only lasts for 1ms at each energy level of the scan there may not be enough counts to drive down the error teams associated with mean velocity or energy.

To accommodate the reduced particle flow through the instrument there are methods to achieve statistically relevant data by alteration to the flight concept of operations. A consideration for the orbit operations would be to integrate for a longer period of time and ultimately achieve a higher number of counts. This is not strictly that straight forward since DANDE will be rotating at 10rpm. Already a 20ms SDEA scan covers a 1° portion of the 360° rotation, so strictly speaking doubling, triple, quadruple, etc. the integration time begins to smear the incoming atmosphere above and below the local horizontal. Consider Figure 9 again there will be some elevation angle of the wind vector with respect to the local horizontal which DANDE is attempting to sense. Where the wind vector is aligned to the instrument boresight will result in the highest magnitude velocity of the particles into WTS by Equation 6 ultimately this will be the peak in energy. It stands to reason then

sampling above and below the wind vector will smear the energy spectrum due to the cosine loss broadening the energy peak causing an ambiguity in the temperature measurements made by the instrument. However, as discussed in [5] there will always be an attitude uncertainty due to the spacecraft spin and discrete integration times.

Alternatively suppose that this energy and angular smear becomes prohibitive there a method where consecutive scans are averaged together ultimately removing the random processes causing counts in the noise floor of the instrument while the true signals remain. This is again not without its own set of issues to overcome. DANDE rotating at 10rpm means that a ram vector scan will not be observed more than 6 seconds apart which spatially would be near 40-45km. The mission objective of DANDE is to provide spatially relevant data on the scale of 10km. With the mind set this is a demonstrator mission it is not prohibitive to average several SDEA scans to achieve a higher signal to noise ratio for the goal of driving down error. Too this end though the reason that averaging over such long length scales can be at issue is the dynamics of the atmosphere may be changing sufficiently to where this is not a relevant course of action. Recall the difference in atmospheric density between a geomagnetic quiet period and a modest active period from Figure 8 the northern hemisphere may be geomagnetically active while the southern hemisphere is quiet. This does not require a change to the flight software of the spacecraft, but rather a rational argument by ground data processing personnel that information content is not being clouded in the data by this process.

Although beyond the scope of this work it is important to consider a key limitation and risk of the WTS instrument as built on the DANDE spacecraft. While counts at the peak may be a key parameter to increase the signal to noise ratio there is an upper bound to the total counts before the supporting circuitry rolls over to zero. For DANDE this roll over ambiguity occurs when the counters reach 256 counts. Integrating longer on each scan does run the risk of rolling over, it could be a calculated risk where the know roll over could be demonstrated to be a set number of integers per scan which could be considered in operations, but this would be the roll over at the peak, not the anodes around the peak. It is undesirable and weights the concept of scan averaging higher in the trade space as a method for reducing measurement error, but cannot go unnoticed.

9.3 Future Instrument Considerations

Simulation through SIMION has proven to be a useful tool for further investigation of the performance of ion optics for the DANDE WTS instrument. As such the results of this line of inquiry have demonstrated the ability to model the physical system of WTS and the data products observed from testing. For future instrument development it is conceivable that preliminary results could be generated through SIMION prior to ever cutting metal and committing to one ion optics design. This is particularly interesting to student programs like DANDE which are financially resource limited and may not be able to afford multiple revisions to an ion optics assembly. The concept of design, model and then test has

the potential to greatly cut the operating cost in the development of an ion optics related instrument.

Having an active as build model at the start of empirical testing will also pay dividends in the course of instrument checkout. The nature of being an ion optics device limits the ability for sensing the performance of the instrument beyond the end to end data capture that would be expected when in full operations. With a readily available model at the beginning of characterizations could change the paradigm presented here where a model is developed in light of testing results. Instead SIMION could help to test a model first and provide baseline performance and operations, then physical unit testing could begin with insight into how the instrument should behave. Not having to take time out of testing to determine the physical processes in play that result in nominal operations, but instead focus on the off nominal testing setup related issues is a potential value added to any program. On a similar vein this process of using SIMION would help to identify observable performance metrics that can be observed by the instrument providing tangible results to carry through testing for comparison.

Bibliography

[1] Binney, James. "Software Model Validation of NMS Instrument." Independent Study. 2011. Print.

[2] Herrero, Fred, et al. *The Gas Kinetic Method for in-situ Satellite Measurements of the Neutral Wind Vector*. Greenbelt, MD, 2008.

[3] Knipp, Delores. *Understanding Space Weather and the Physics Behind it*. McGraw Hill Learning Solutions, 2011. Text.

[4] Pilinski, Marcin and Palo, Scott. *Monte Carlo Modeling of an In-Situ Particle Detector with a Small Deflection Energy Analyzer*. DANDE Internal. Boulder, CO: Unpublished, 2011.

[5] Pilinski, Marcin D. *Analysis of a Novel Approach for Determining Atmospheric Density from Satellite Drag*. Thesis. University of Colorado Boulder. Ann Arbor: UMI Dissertation Services, 2008. Print.

[6] Sutton, Eric. *Effects of Solar Disturbances on the Thermosphere Densities and Winds from CHAMP and GRACE Accelerometer Data*. PhD Thesis. Boulder: University of Colorado at Boulder, 2008.

[7] Herrero, Fred. "Light-Trap Design Using Multiple Reflections and Solid-Angle Attenuation: Application to a Spaceborne Electron Spectrometer." *Applied Optics* 31.25 (1992): 5331-340. *Optical Society of America*.

[8] "UN5-NMS200.1." *NMS Master Assembly*. Boulder, CO, December 2008.